

Learning to Rank Ace Neural Architectures via Normalized Discounted Cumulative Gain

Yuge Zhang¹ Quanlu Zhang¹ Li Lyna Zhang¹ Yaming Yang¹ Chenqian Yan² Xiaotian Gao¹ Yuqing Yang¹

Abstract

One of the key challenges in Neural Architecture Search (NAS) is to efficiently rank the performances of architectures. The mainstream assessment of performance rankers uses ranking correlations (*e.g.*, Kendall’s tau), which pay equal attention to the whole space. However, the optimization goal of NAS is identifying top architectures while paying less attention on other architectures in the search space. In this paper, we show both empirically and theoretically that Normalized Discounted Cumulative Gain (NDCG) is a better metric for rankers. Subsequently, we propose a new algorithm, AceNAS, which directly optimizes NDCG with LambdaRank. It also leverages weak labels produced by weight-sharing NAS to pre-train the ranker, so as to further reduce search cost. Extensive experiments on 12 NAS benchmarks and a large-scale search space demonstrate that our approach consistently outperforms SOTA NAS methods, with up to 3.67% accuracy improvement and 8× reduction on search cost.

1 Introduction

Neural Architecture Search (NAS) has shown its effectiveness on various tasks (Howard et al., 2019; Tan & Le, 2020; So et al., 2019). Its core idea is to automatically design suitable network architectures for a given dataset. Although early NAS (Zoph & Le, 2016) is successful in outperforming human-designed models, its computational cost can be prohibitive, because it takes up to 1,800 GPU days to train thousands of architectures. Such excessive training cost motivates the followed-up works to develop efficient strategies to estimate the rankings of architecture performances. A reliable *performance ranker* (Elsken et al., 2018; White et al., 2021) is known to be a key component in NAS to help quickly filter out the bad-performing architectures and

*Equal contribution ¹Microsoft Research ²Xiamen University, work done as an intern at MSRA. Correspondence to: Yuge Zhang <Yuge.Zhang@microsoft.com>.

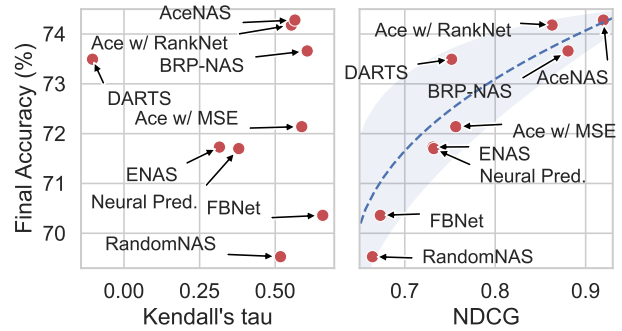


Figure 1: We evaluate KdT, NDCG and final NAS performance of 11 rankers. **(Left)** Better KdT does not necessarily yield better accuracy. **(Right)** NDCG and accuracy are clearly positively correlated.

identify the best.

This paper firstly concerns the assessment of performance rankers. Other than reporting the performance of final searched architecture, many works (White et al., 2021; Wen et al., 2020; Pourchot et al., 2020; Dong & Yang, 2020; Zhao et al., 2021; Guo et al., 2020) have used ranking correlations like *Kendall’s tau* (*KdT*), to demonstrate the robustness of their method, or to achieve a deeper understanding. Although widely used, whether such metric is actually eligible to assess a ranker’s quality remains in doubt. To answer this question, we curate 11 state-of-the-art NAS performance rankers from NNI (Zhang et al., 2020a) as well as AceNAS (described below), and measure their KdT and final accuracy on NAS-Bench-201. The result, shown in the left figure of Figure 1, is surprising: (i) the worst and the best ranker both have KdT around only 0.5, yet their final accuracy differ a lot; (ii) although some rankers have poor KdT, their final accuracy can be still very competitive. These observations suggest that KdT is not a good assessment metric in NAS, which we believe might mislead research directions.

We identify one of the reasons why KdT is not a good metric to be, KdT pays equal attention to all the architectures in search space. It can not reflect the effectiveness of a ranker when it is used in a NAS experiment, which only cares about the top-tier architectures. Recently, we notice another popular ranking metric named *Normalized Discounted Cumulative Gain* (*NDCG*). Unlike KdT which considers ev-

ery ranked items equally, *NDCG* attaches larger weights to the best items, thus gives more attention to most important items. *NDCG* is widely used to assess *Learning to Rank (LTR)* algorithms in Information Retrieval (IR) community. Inspired by this, it is intuitive to ask *can we apply NDCG in NAS to better rank top-performing architectures?*

Despite the success of *NDCG* in IR (Liu, 2011), we face two major challenges when using *NDCG* to find top-performing architectures in NAS. Firstly, *NDCG* was initially designed for document ranking problems. The applicability of *NDCG* in NAS is only an intuition, which lacks theoretical and empirical support. Secondly, since it is time-consuming to obtain the train-from-scratch accuracy of a neural network, it is challenging to efficiently get a large number of architectures’ accuracies to optimize the *NDCG* in NAS.

To tackle the above challenges, we first show that *NDCG*, with careful adaptation, is a good metric for performance rankers in NAS. This is proved both theoretically and empirically. We then propose a novel algorithm called AceNAS. We utilize LambdaRank (Borges et al., 2007), a list-wise LTR approach, to directly maximize *NDCG* of a ranker. To reduce the time cost of computing ground-truth architecture-accuracy pairs, we leverage the weak supervision obtained from weight-sharing NAS. Though the rank obtained with weight sharing is not accurate (Niu et al., 2020), it contains implicit semantics of architectures (Zhang et al., 2020c) that is helpful for down-streaming tasks (e.g., accuracy prediction) if used properly. To the end, AceNAS is a two-stage algorithm, where we first pre-train the ranking model on massive number of inaccurate but easily-obtained weight-sharing labels, and then fine-tune the ranker with only a small number of fully-trained models’ accuracies with LambdaRank.

We conduct extensive experiments on 12 combinations of search spaces and datasets with benchmarks and ProxylessNAS search space (Cai et al., 2019b). The results demonstrate that AceNAS consistently outperforms the SOTA performance ranker. Specifically, we achieve a same-level accuracy with only 110 ground-truth architectures on NAS-Bench-101 (Ying et al., 2019), which reduces the search cost by $18\times$ than GBDT-NAS (Luo et al., 2020a), $8\times$ than SemiNAS (Luo et al., 2020b) and BONAS (Shi et al., 2020). On NAS-Bench-201 (Dong & Yang, 2020), we achieve an improvement of up to 3.67% in accuracy under similar cost. On ProxylessNAS (Cai et al., 2019b), AceNAS achieves SOTA under mobile settings (ImageNet top-1 75.13%, 84ms). Remarkably, AceNAS surpasses two GCN-based accuracy predictors on all the benchmarks with even smaller costs.

To sum up, our main contributions are listed as follows:

- We advocate *NDCG* as a new metric of performance rankers in NAS, and prove its effectiveness both theoretic-

cally and empirically.

- We propose a novel algorithm, AceNAS, which directly optimizes *NDCG*, and leverages weight sharing as weak labels to accelerate the search process.
- We comprehensively evaluate and demonstrate superiority of our approach over state-of-the-art methods on various search spaces and datasets. We will open-source the whole code base to facilitate future NAS research.

2 Related works

Performance rankers in NAS. We focus on performance estimation strategy in NAS. In this paper, we call them *performance rankers*, because as pointed out by (Elsken et al., 2018), for most of the times only relative rankings matter. One popular method is called weight sharing (Pham et al., 2018; Liu et al., 2018; Wu et al., 2019; Cai et al., 2019b). It creates a super-net which contains all the architectures in the search space, such that every possible architecture is a sub-net. Then sub-net’s accuracy is used to estimate its accuracy when trained alone. Although it can save the cost to train each architecture from scratch, its effectiveness is still a question under debate (Yu et al., 2019; Li & Talwalkar, 2019; Zhang et al., 2020b; Bender et al., 2020). Recently, another method called “performance predictor” (Baker et al., 2017; Dai et al., 2018; Chau et al., 2020; Wen et al., 2020) is gaining popularity. It collects data-points of architecture-accuracy pairs, and trains a ranking model in a supervised learning manner. Although it outperforms weight-sharing on many benchmarks, the cost of collecting enough data-points remains high. Aiming to take the best of both worlds, we combine these two approaches in our design.

Assessment metrics for performance rankers. The ideal and intuitive evaluation of performance rankers is to integrate it with a search strategy and conduct a search on a particular space. However, as argued by (Yu et al., 2019), such evaluation is coupled with many factors such as sampling strategy, making fair comparison under controlled settings difficult. Moreover, since only the best model of the search process is reported, the ranker’s robustness is not reflected in the evaluation. On the other hand, literature often adopts ranking correlations (e.g., KdT) that shows the consistency between the predicted rank and ground-truth rank (Yu et al., 2019; Pourchot et al., 2020; Zhang et al., 2020b; Yu et al., 2020; White et al., 2021). The wide usage of ranking correlations has even catalyzed recent works (Xu et al., 2021; Chau et al., 2020) that directly minimizes ranking errors. However, correlation metrics neglect the fact that the goal of NAS is to find top-performing architectures in the search space. Treating all the architectures equally is not well aligned with such goal, resulting in less efficient algorithms. Therefore, we advocate *NDCG* that takes

the full ranking list into consideration but also emphasizes top-performing architectures.

Learning to Rank and Information Retrieval. Learning to rank (LTR) (Liu, 2011) uses machine learning technologies to build effective ranking models, and is widely used in solving document ranking problem in Information Retrieval (IR). We come to notice LTR because NAS is also trying to solve a ranking problem. Over the past decades, many LTR methods have been proposed and deployed in modern IR systems like search engines. They can be categorized into pointwise (Crammer & Singer, 2001; Cooper et al., 1992), pairwise (Burgess et al., 2005; Tsai et al., 2007) and listwise (Burgess et al., 2007). Our method relies on LambdaRank, which falls into the category of listwise approaches.

3 NDCG: a new metric for rankers in NAS

3.1 Problem formulation

The NAS problem can be formulated as,

$$\alpha^* = \arg \max_{\alpha \in \mathcal{A}} \text{ACC}(\alpha) \quad (1)$$

which is finding the architecture from a search space \mathcal{A} , $\alpha \in \mathcal{A}$, such that $\text{ACC}(\alpha)$ (*i.e.*, ground-truth accuracy¹ of α) is maximized. Since obtaining the precise $\text{ACC}(\alpha)$ requires fully training a neural network, which is costly, previous works often design a performance ranker f , and use $f(\alpha)$ as a proxy of $\text{ACC}(\alpha)$.

Focusing on performance rankers, we first introduce the notations we will use throughout the rest of this paper. Let $\mathbf{a} = \{\alpha_1, \alpha_2, \dots, \alpha_n\}$ be the architectures to rank, whose ground-truth accuracy is $\mathbf{acc} = \{\text{acc}_1, \text{acc}_2, \dots, \text{acc}_n\}$ respectively. The performance ranker is $f : \mathcal{A} \rightarrow \mathbb{R}$, *i.e.*, a ranking function f in function space \mathcal{F} . $\pi_f(i)$ ($1 \leq i \leq n$) is the ranked list produced by f , such that $f(\alpha_{\pi_f(1)}) \geq f(\alpha_{\pi_f(2)}) \geq \dots \geq f(\alpha_{\pi_f(n)})$.

With the formulations above, Equation (1) can be written as the following bi-level optimization:

$$\begin{aligned} \alpha^* &= \arg \max_{\alpha \in \mathcal{A}} f^*(\alpha) \\ \text{s.t. } f^* &= \arg \max_{f \in \mathcal{F}} \text{OBJECTIVE}(f) \end{aligned} \quad (2)$$

One of the challenges in this optimization is to find a good $\text{OBJECTIVE}(\cdot)$ to guide the optimization of f . We identify two essential properties of rankers that a good objective should encourage. (i) $\arg \max f^*(\alpha)$ and $\arg \max \text{ACC}(\alpha)$ should be as close as possible, which means the ranker

should precisely predict the top-tier architectures’ ranking. (ii) As \mathcal{A} is often large and solving $\arg \max f^*(\alpha)$ requires optimization techniques, it should also give reasonable rankings to worse architectures to hint the “argmax optimizer” to find global maximum. Existing widely used objectives (*e.g.*, minimizing pairwise ranking errors) (Xu et al., 2021) often satisfy property (ii) but neglect property (i).

Property (i) is critical for identifying the best among good performing architectures. To possess this property, we resort to NDCG, a renowned ranking metric in Information Retrieval, as the objective, which satisfies the two properties mentioned above simultaneously. This design choice is inspired by the observation that NAS has similar optimization goal to IR. In IR, when retrieving the best matched documents from a large number of documents, the ranking quality of high relevant documents is more important than that of low relevant documents. Similarly in NAS, model developers care more about identifying the top architecture from those relatively good-performing models, while distinguishing which one is worse among bad-performing models is less important.

3.2 Normalized Discounted Cumulative Gain

Normalized Discounted Cumulative Gain (NDCG) (Järvelin & Kekäläinen, 2002), which has been proved effective and has been widely adopted in IR (Liu, 2011), is a metric of ranking quality and is often used to measure effectiveness of a ranker. It properly shifts the focus of the ranking towards the front part of the rank. It takes into account the graded relevance values and encourages the highly relevant items to come up into the top of recommended lists. In the context of NAS, with the notation given in Section 3.1, NDCG can be computed as,

$$\text{NDCG}(f; \mathbf{a}, \mathbf{r}) = \frac{\sum_{i=1}^n \frac{1}{\log_2(i+1)} (2^{r_{\pi_f(i)}} - 1)}{\sum_{i=1}^n \frac{1}{\log_2(i+1)} (2^{r_i} - 1)} \quad (3)$$

where the numerator is often written as $\text{DCG}(f; \mathbf{a}, \mathbf{r})$ and the denominator is known as IDCG (Ideal DCG) because it is the DCG with f as a perfect ranker. $\mathbf{r} = \{r_1, r_2, \dots, r_n\}$ ($0 \leq r_i \leq S$) are relevance scores which are proportional to accuracy. Hence, NDCG is the normalized DCG in $[0, 1]$. If a model with high accuracy gets ranked poorly, DCG gets penalized. The “ 2^{r_i} ” part emphasizes on models with higher accuracy, thus encourages the ranker to retrieve more of them, rather than focusing equally on the whole rank.

The architectures’ accuracy should be properly mapped to the relevance score. Specially in NAS, the distribution of accuracy is usually highly skewed, *i.e.*, the values span in the whole range while most of them gather in a much smaller range. Simply normalizing the whole distribution to the range (*e.g.*, 0-10) used in IR will not work. For instance, when dealing with a long-tail distribution with most

¹We will use “accuracy” for short throughout this paper. Note that test accuracy can be easily replaced with other metrics. We use the term “ground-truth accuracy” to denote the test accuracy when the model is fully trained.

architectures’ accuracy above 90% and a few additional low-accuracy outliers, using min-max normalization vanishes the ability of distinguishing the accuracy of most architectures. Therefore, we compute new lower and upper bound to clip the distribution. Due to the exponential effect of “ 2^{r_i} ”, the distribution should be scaled to a proper range (*i.e.*, relevance scale S) to maximize the effectiveness of identifying top architectures. The empirical study of the clipping and scaling is detailed in Appendix B.1.3.

3.3 Analysis of NDCG in the context of NAS

Equation (3) implies that the ranking focus is skewed towards the front part of the rank, which properly balances the ability of discriminating good-performing architectures and the ability of distinguishing good architectures from bad ones. As a metric (*e.g.*, NDCG) of a performance ranker should eventually serve the final goal of NAS, it is necessary to prove the alignment between the metric and the final goal. In NAS, *top-k accuracy* is a widely recognized metric to reflect how well the final goal is achieved (Wen et al., 2020; Bender et al., 2018; Mellor et al., 2020). Specifically, *top-k accuracy* is computed by evaluating the ground-truth accuracy of top k architectures indicated by the ranker and pick out the best one from them. Below, we prove the correlation between NDCG and *top-k accuracy* theoretically, then use empirical study to illustrate the property and effectiveness of NDCG.

3.3.1 THEORETICAL ANALYSIS

Definition 3.1. Consider a scenario where the ranker f selects k ($1 \leq k \leq n$) models with highest prediction scores from $\mathbf{a} = \{\alpha_1, \alpha_2, \dots, \alpha_n\}$ and fully trains them. With the budget k , the final NAS performance is defined as,

$$\text{TopK}(f; \mathbf{a}, \mathbf{r}, k) = \max_{1 \leq i \leq k} r_{\pi_f(i)}.$$

Here we used relevance scores instead of accuracy. As they are proportional, the conclusions are similar.

Theorem 3.2. If $\text{NDCG}(f; \mathbf{a}, \mathbf{r}) \geq \nu$ and $k > (n+1) - (n+1)^\nu$, $\text{TopK}(f; \mathbf{a}, \mathbf{r}, k) \geq \nu \left(\frac{\sum_{i=1}^n r_i c_i}{\sum_{i=1}^n c_i} \right)$, where,

$$c_i^{(\nu, k)} = \begin{cases} \frac{1}{\log_2(i+1)} - \frac{1}{\nu \log_2(i+k+1)} & \text{if } 1 \leq i \leq n-k \\ \frac{1}{\log_2(i+1)} & \text{if } n-k < i \leq n \end{cases}$$

In Theorem 3.2, $h(\nu) = \nu \left(\frac{\sum_{i=1}^n r_i c_i}{\sum_{i=1}^n c_i} \right)$ is an increasing function of ν (proved in Appendix D). Thus, TopK is lower bounded by a function that is monotonically increasing to NDCG.

Theorem 3.3. Assume two rankers f_1 and f_2 are randomly drawn from \mathcal{F} , $n \gg K$. Let $\text{TopK}(f_1; \mathbf{a}, \mathbf{r}, k) \geq r_{t_1}$, $\text{TopK}(f_2; \mathbf{a}, \mathbf{r}, k) \geq r_{t_2}$. If $r_{t_1} > r_{t_2}$ and $r_{t_1}, r_{t_2} \geq \log_2 \left(\frac{1}{n} \sum_{i=1}^n 2^{r_i} \right)$, $\mathbb{E}[\text{NDCG}(f_1; \mathbf{a}, \mathbf{r})] > \mathbb{E}[\text{NDCG}(f_2; \mathbf{a}, \mathbf{r})]$ holds.

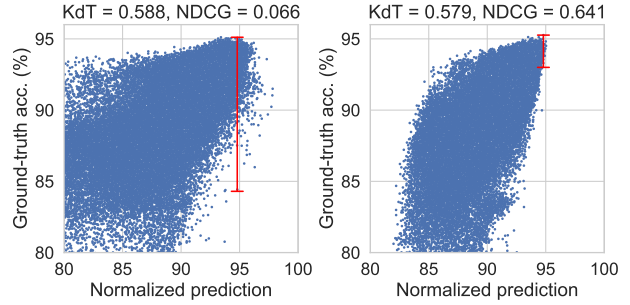


Figure 2: The prediction – ground-truth scatter plot of two rankers. The two rankers have identical network structures. **(Left)** Ranker optimized for KdT and the top-1 accuracy based on it is 90.98%. The red line marks the region where the ranker gives high scores but its ground-truth accuracy are low. **(Right)** Ranker is optimized for NDCG and the top-1 accuracy based on it is 94.51%.

Further, Theorem 3.3 proves that a ranker with better TopK is expected to have a higher NDCG. The full proof is detailed in Appendix D.

3.3.2 EMPIRICAL ANALYSIS

One experiment is to illustrate the correlation between prediction accuracy and ground-truth accuracy in Figure 2, where the prediction accuracy is produced by optimizing KdT and NDCG respectively (see next section). The two accuracy rankers have identical structures (Wen et al., 2020). When the ranker is trained to maximize KdT (*i.e.*, full-ranking correlation (Chau et al., 2020; Xu et al., 2021)), the final KdT of the prediction accuracy is 0.588 as shown in the left figure. However, the architectures with 95% predicted accuracy have varied ground-truth accuracy between 85% and 95%. In contrast, the ranker optimized for NDCG has a much sharp head (*i.e.*, top right of the right figure), the architectures with 95% predicted accuracy are precisely located in a much smaller range (*i.e.*, 93%-95%) of the ground-truth accuracy. Besides, this ranker produces equally good KdT (*i.e.*, 0.579), which means it is also qualified to distinguish good architectures from bad ones.

To further demonstrate the effectiveness of NDCG, we collect rankers from 12 search spaces (listed in Section 5) and pairwise compare them. Suppose we have m search spaces, and for the i -th search space, we get d_i rankers $f_{i,1}, f_{i,2}, \dots, f_{i,d_i}$. In total, we get $\sum_{i=1}^m \frac{d_i(d_i-1)}{2}$ ranker pairs. In this experiment, $m = 12$ and we get 486 ranker pairs in total. For each pair $f_{i,j}, f_{i,k}$, we determine whether the ranker with higher NDCG also produces better top- k test accuracy. If it does, we count this pair as a “successful” distinguished ranker pair for NDCG. Then for each k , we compute “success rate”, which is number of successful distinguished pairs divided by total number. The success rate is similarly computed for ranking correlations including Kendall’s tau and Spearman’s rho. We also include top-1,

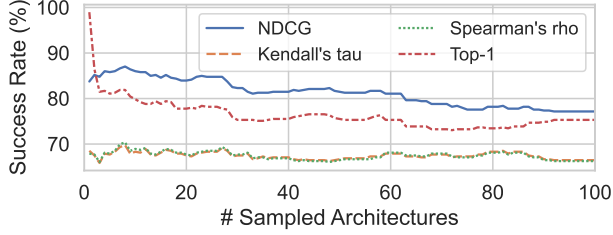


Figure 3: Comparison of the success rate with four different ranking metrics. k sampled architectures use top- k to evaluate success rate.

i.e., the accuracy of architecture with the highest prediction score, into comparison.

Results are shown in Figure 3. There are two findings: (i) NDCG can distinguish a good ranker from a poor one with more than 80% probability, which is much higher than correlations like KdT. (ii) The success rate of NDCG even surpasses top-1 under various budgets. This is because top-1 only takes the highest prediction into account and it might not be robust enough to comprehensively assess a ranker’s quality, which echoes the argument in (Yu et al., 2019).

More empirical analysis are in Appendix E.1.1.

4 AceNAS: Learning to Rank Ace Architectures

Once we set up NDCG as a new metric to evaluate NAS performance rankers, a natural follow-up idea is to directly optimize NDCG of performance rankers. By incorporating techniques from information retrieval, we show that direct optimization of NDCG is feasible with LambdaRank. Meanwhile, to make our algorithm more practical, we pre-train the ranker with weak labels obtained from a well-trained super-net to greatly reduce architecture-accuracy pairs needed.

The overall illustration of AceNAS is shown in Figure 4, which is divided into two stages. First, pre-training a GCN-based ranker with weakly supervised labels from a well-trained super-net. Second, transferring the pre-trained GCN into another ranker and fine-tuning it with LambdaRank with limited architecture-accuracy pairs.

4.1 LambdaRank

We follow (Wen et al., 2020; Chau et al., 2020) to design a ranker with GCN (Kipf & Welling, 2016), that takes a neural network architecture as input and predicts its score. It first encodes neural architectures into an encoding with a few graph convolutional layers, then use a ranking head (*i.e.*, a Multi-layer perceptron) to output the prediction. Detailed designs can be found in Appendix B.1.4. To train the ranker, we follow the state-of-the-art paradigm – performance predictors (Wen et al., 2020) – to collect a number

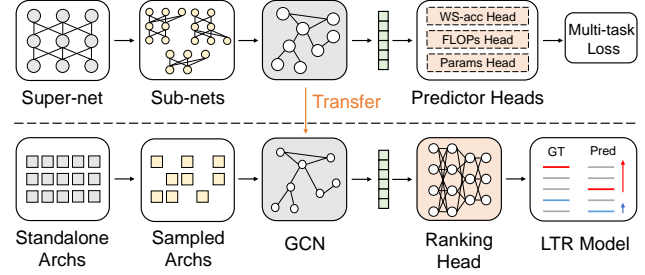


Figure 4: **(Top)** AceNAS first samples weak labels on super-net to train the ranking model with multi-task loss. **(Bottom)** The trained GCN is transferred to optimize the LTR model.

of data-points, *i.e.*, pairs of architecture and accuracy. Next, we describe how the optimization is done.

Suppose we have a ranker f_ω parameterized with ω and a set of known architecture-accuracy pairs $\{(\alpha_1, \text{acc}_1), \dots, (\alpha_m, \text{acc}_m)\}$. Let $\{r_1, r_2, \dots, r_m\}$ be their corresponding relevance (see Section 3.2). The optimization goal can be formally written as,

$$\omega^* = \arg \max_{\omega} \text{NDCG}(f_\omega; \{\alpha_1, \dots, \alpha_m\}, \{r_1, \dots, r_m\}) \quad (4)$$

LambdaRank (Burgess et al., 2007), a well reputed LTR algorithm, is capable of optimizing Equation (4). At its core part, gradients can be directly computed with LambdaRank without actually computing the loss explicitly. Specifically, for a pair (α_i, α_j) whose ranking score is $(f_\omega(\alpha_i), f_\omega(\alpha_j))$ and $r_i > r_j$, the gradient of ranking model parameter ω is computed as,

$$\frac{\delta \mathcal{L}}{\delta \omega} = \lambda_{ij} \left(\frac{\delta f_\omega(\alpha_i)}{\delta \omega} - \frac{\delta f_\omega(\alpha_j)}{\delta \omega} \right) \quad (5)$$

$$\lambda_{ij} \equiv \frac{-\sigma}{1 + e^{\sigma(f(\alpha_i) - f(\alpha_j))}} |\Delta_{\text{NDCG}}| \quad (6)$$

σ is the hyper-parameter controlling the shape of sigmoid. $|\Delta_{\text{NDCG}}|$ measures the change of NDCG if the ground-truth ranking position of α_i and α_j get swapped. Swapping higher ranked items gets more penalty, leading to a larger gradient. Note that if $|\Delta_{\text{NDCG}}|$ is replaced with 1, Equation (5) reduces to RankNet (Burgess et al., 2005), which minimizes the number of inversions in the full ranking.

4.2 Weak supervision of weight sharing

To reduce the required number of architecture-accuracy pairs and make the algorithms more practical, we propose to use weak supervision from a well-trained super-net (*i.e.*, accuracy evaluated using the weights from super-net) to pre-train the ranker. A super-net is trained with weight sharing approach (single-path random sampling (Li & Talwalkar, 2019; Guo et al., 2020) in our experiments), and thus the computation cost is comparable to training a single architecture. The design of treating weight sharing accuracy as

weakly supervised labels is inspired by the observation in previous research (Zhang et al., 2020c) that weight sharing super-net is capable of differentiating good architectures from bad ones, with relatively high ranking correlation.

To empower our ranker with knowledge from super-net, we replace ranking head in the ranker with a *WS-accuracy head* in the pre-training. The ranker is trained with mean-squared-error (MSE) loss instead of using LambdaRank, because weight sharing labels are not qualified for identifying the best architectures from good-performing ones. To further boost the effectiveness of pre-training, inspired by (Dai et al., 2020; Chau et al., 2020), we incorporate multi-task training by introducing additional two heads that predict FLOPs and number of parameters respectively. The ranker is trained to minimize the following multi-task mean-squared-error (MSE) loss:

$$\begin{aligned} \mathcal{L}_{\text{pretrain}} = & \mathcal{L}_{\text{mse}}(\text{acc}_i, \text{acc}_i^*) + \lambda_1 \cdot \mathcal{L}_{\text{mse}}(\text{flops}_i, \text{flops}_i^*) \\ & + \lambda_2 \cdot \mathcal{L}_{\text{mse}}(\text{params}_i, \text{params}_i^*) \end{aligned} \quad (7)$$

where variables marked with stars (*) are predictions.

5 Evaluation

5.1 Experiment setup

Search space. We evaluate AceNAS on both the NAS benchmarks and the widely-used ProxylessNAS (Cai et al., 2019b) search space.

- *NAS Benchmarks.* We collect 12 benchmarks (10 different search spaces, and 3 different datasets) from NAS-Bench-101 (Ying et al., 2019), NAS-Bench-201 (Dong & Yang, 2020) and NDS (Radosavovic et al., 2019). Each benchmark provides the ground-truth accuracy for every architecture, so that a comprehensive evaluation of our method is computationally feasible.
- *ProxylessNAS.* We also measure AceNAS on a large chain-wise search space that consists of 21 sequential MB-Conv searchable blocks. Unlike NAS Benchmarks, the search space is much larger (i.e., 2.58×10^{17} candidates) and there is no ground-truth accuracy for candidate architectures. To be comparable with ProxylessNAS-mobile, we follow (Bender et al., 2020) and use a same latency lookup table to constrain the search space within 83ms – 85ms.

Algorithm details. Our first step is to get the three weak labels (i.e., validation accuracy from weight-sharing NAS, FLOPs, and parameter size). We encode the full search space into a super-net and adopt the widely-used uniform random sampling approach (Guo et al., 2020) to train the super-net. Based on the trained super-net, we randomly sample 4k architectures and obtain weak labels. The sampled

Table 1: Comparison with SOTA NAS methods. Budget here refers to the number of fully-trained architectures. † We reproduced BRP-NAS using FLOPs for pre-training.

Method	NAS-Bench-101		NAS-Bench-201	
	Budget	Test Acc.	Budget	Test Acc.
Oracle	423,624	94.34	15,625	73.48
Random	1,000	93.42	100	69.94
GBDT-NAS (Luo et al., 2020a)	2,000	94.14	-	-
SemiNAS (Luo et al., 2020b)	2,000	94.02	-	-
RE (Real et al., 2019)	1,000	93.72	100	70.69
RL (Zoph & Le, 2016)	1,000	93.58	100	70.68
BOHB (Falkner et al., 2018)	1,000	93.72	100	69.71
BONAS (Shi et al., 2020)	1,000	94.24	-	-
Unsup. encoding (Yan et al., 2020)	400	94.10	-	73.37
GA-NAS (Rezaei et al., 2021)	1561	94.23	444	73.28
ReNAS (Xu et al., 2021)	423	93.95	90	72.12
Neural Predictor (Wen et al., 2020)	219	94.04	-	-
BRP-NAS (Chau et al., 2020) †	110	94.05	110	72.79
AceNAS	110	94.10	110	73.38
AceNAS (small)	30	93.92	30	72.04
AceNAS (large)	1,000	94.32	500	73.47

architectures and their weak labels are used for the ranker pre-training. The second step is to fine-tune the ranker with train-from-scratch accuracy labels. AceNAS spawns trials and collects their fully-trained accuracy (this can be a table lookup if a benchmark is available) to train the ranker with LambdaRank. This step is repeated a few times with the *iterative sampling* strategy (Chau et al., 2020). Finally, we use the fine-tuned ranker to predict best-performing architectures from the search space. A formal description of the algorithm workflow is included in Appendix C.

Evaluation metrics. We use **budget** to refer to the total number of architectures fully-trained in iterative sampling and final model selection. **Test accuracy** is used as an end-to-end metric, which is the test accuracy (after fully-trained) of the best model ever encountered during the whole search process. To purely assess the quality of a ranker, we use **top-k test accuracy** (Yu et al., 2020), in which, we train and evaluate k (e.g., $k = 10$ in NAS benchmarks) architectures top-ranked by the ranker, and get the test accuracy of the best one. **Test regret** (Ying et al., 2019) is to measure the test accuracy gap between the best model found by NAS and the best one in the search space. Notably, we assume the test dataset is invisible during search. Therefore, we always select model on validation dataset and report its accuracy on test dataset.

5.2 AceNAS on NAS benchmarks

Comparison with state-of-the-art methods. We first evaluate AceNAS by comparing to prior works on NAS-Bench-101 and 201 (CIFAR-100). We list out the results in Table 1, where we run each method on each benchmark 50 times. To evaluate the effectiveness of our work, we set three different levels of budgets (i.e., 30, 110, and 1000 fully-trained architectures). Note that AceNAS has an extra weight sharing stage, but its cost is comparable to fully train 2 – 3 architec-

Table 2: Comparisons of test accuracy by different GCN-based approaches on 12 benchmarks (10 search spaces and 3 datasets).

Benchmark	Vanilla	BRP	AceNAS
NAS-Bench-101	93.60	94.05	94.10
NAS-Bench-201 (CIFAR-10)	94.10	94.35	94.52
NAS-Bench-201 (CIFAR-100)	71.96	72.93	73.38
NAS-Bench-201 (ImageNet)	45.70	46.31	46.34
NDS-Amoeba	94.73	94.85	94.84
NDS-DARTS	94.84	94.88	94.92
NDS-DARTS-fix-w-d	94.01	94.12	94.16
NDS-ENAS	94.78	94.91	94.97
NDS-ENAS-fix-w-d	93.94	94.05	94.13
NDS-NASNet	94.76	94.92	95.02
NDS-PNAS	94.95	94.99	95.06
NDS-PNAS-fix-w-d	94.23	94.27	94.34

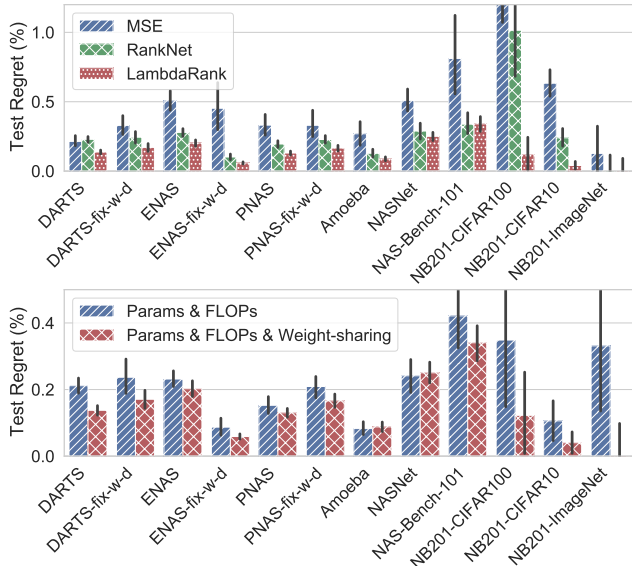


Figure 5: Comparison among test regrets when using different LTR loss (**top**) and when pre-training with different labels (**bottom**). Budget is fixed to 110.

tures, which is negligible. The budget is split into 5 rounds of iterative sampling, and we sample another 10 architectures at last, for budget 30 and 110. Compared to previous works, we achieve a comparable accuracy with only 110 ground-truth accuracy labels on NAS-Bench-101. This cost is $18\times$ smaller than GBDT-NAS, and $8\times$ smaller than RE, RL, BOHB, SemiNAS and BONAS. On NAS-Bench-201, we achieve 0.59% – 3.67% higher accuracy when the same number of ground truths are sampled. We further decrease the budget and find that, even with a budget as small as 30, AceNAS is still competitive with several baselines. Notably, when we increase budget to 1,000 on NAS-Bench-101 and 500 on NAS-Bench-201, AceNAS significantly outperforms other baselines. It achieves similar accuracy with the best architecture (oracle), with only 0.02% and 0.01% gap on

NAS-Bench-101 and NAS-Bench-201, respectively. This result indicates that AceNAS can achieve fast convergence without sacrifice of final performance.

Comparison with GCN-based approaches on different search spaces. We then further demonstrate the effectiveness of AceNAS on other search spaces. We implement two most related GCN-based approaches on all benchmarks: (i) Vanilla, a basic GCN predictor proposed in (Wen et al., 2020) and (ii) BRP-NAS, a state-of-the-art binary-relation predictor that also leverages FLOPs and latency in pre-training. The results (when budget = 110) are shown in Table 2. AceNAS outperforms baselines on 11 out of 12 benchmarks. We demonstrate a more detailed comparison under different budgets in Appendix E.2 and Appendix E.3.

5.2.1 ABLATION STUDY ON NAS BENCHMARKS

LambdaRank vs. other ranking loss. We compare LambdaRank with MSE loss and RankNet loss. MSE loss is employed in Neural Predictor (Wen et al., 2020). RankNet (Burges et al., 2005) loss is essentially the same as LambdaRank but does not take into account the changes in NDCG and treat all architecture-accuracy pairs equally (as discussed in Section 4.1). As shown in Figure 5 (**top**), on all search spaces, AceNAS with optimizing LambdaRank loss achieves much smaller test regrets than MSE and RankNet. We further conduct comparisons in Appendix E.4 to demonstrate that LambdaRank loss is consistently outperforming the other two under different pre-training settings.

Weak labels. We then evaluate the effectiveness of using weight sharing labels to pre-train GCN. Our comparison baseline is *Parameters & FLOPs*, that removes weight sharing from AceNAS (i.e., *Params. & FLOPs & Weight-sharing*). Figure 5 (**bottom**) shows the test regrets on 12 search spaces and datasets. With the weak supervision of weight sharing labels, we significantly reduce the test regret by up to 0.39%.

5.2.2 ACENAS UNDER VARIOUS WEIGHT SHARING METHODS

The previous experiment demonstrates that weak supervision by single-path weight sharing (Guo et al., 2020) can improve the search accuracy of AceNAS. Then, the question naturally arises: does the quality of weak supervision impact the effectiveness of AceNAS? To verify this, we conduct experiments with various weight sharing methods in state-of-the-art NAS works.

Table 3 summarizes the results on two search spaces. To measure the quality of various weak supervision methods, we train the super-net with various weight sharing methods (e.g., Gradient and RL). Then, we retrain the top 10 architectures indicated by the weight sharing method, and use the best accuracy as the method’s quality. As shown

Table 3: Top-10 accuracy of AceNAS under various weight-sharing methods. “NDS-DARTS” is abbr. for NDS-DARTS-fix-w-d. The maximum value in each column is bold, and the minimum is underlined.

WS strategy	Search method	NAS-Bench-201 space		NDS-DARTS space	
		WS quality	AceNAS	WS quality	AceNAS
RandomNAS	Single-path	93.16	94.52	93.52	94.16
DARTS (1st order)	Gradient	94.45	94.57	94.14	94.30
DARTS (2nd order)	Gradient	<u>84.60</u>	94.46	93.80	94.12
FBNet	Gradient	93.96	94.51	<u>93.50</u>	<u>94.10</u>
ProxylessNAS	Gradient/RL	87.43	<u>94.44</u>	93.65	94.16
ENAS	RL	93.67	94.50	94.01	94.12

Table 4: Top-1 ImageNet accuracy on ProxylessNAS search space. †: accuracy numbers are from the original papers.

	Test Acc. (%)	Latency (ms)
TuNAS (Bender et al., 2020) [†]	75.0	84.0
ProxylessNAS (Cai et al., 2019b) [†]	74.6	84.4
MnasNet-B1 (Tan et al., 2019) [†]	74.5	84.5
Neural Predictor (Wen et al., 2020)	74.75	84.95
AceNAS	75.13	84.59

in Table 3, when equipped with a better weight sharing method, AceNAS can be even better. Remarkably, by applying the weak supervision of DARTS (1st order), AceNAS achieves 94.57% and 94.30% test accuracy on NAS-Bench-201 (oracle: 94.57%) and NDS-DARTS-fix-w-d (oracle: 94.32%), respectively, which are close to the best in the whole search space. Besides, although DARTS (2nd order) and ProxylessNAS have a much weaker supervision on the NAS-Bench-201 search space, AceNAS can still find good-performing architectures. This suggests that AceNAS is robust to low-quality weak supervision. More results can be found in Appendix E.5.

5.3 AceNAS on ProxylessNAS search space

We now evaluate AceNAS on the large chain-wise search space in ProxylessNAS. We integrate AceNAS into a evolutionary search algorithm (Real et al., 2019) by replacing its fitness function with the output of our performance ranker. The evolution is splitted into 5 stages, where the population size of first stage is 80, and each of the rest stages has 30 individuals. A weight-shared super-net is trained before the first stage begins, which produces weak labels to pre-train the ranker, and the ranker is fine-tuned at the end of each stage. Architecture training recipes follow the same settings in (Bender et al., 2020).

Table 4 lists out the results. Compared to state-of-the-art NAS methods on ProxylessNAS search space, AceNAS reaches the highest test accuracy of 75.13% (an average over 3 runs that report 75.29%, 75.09%, 75.00% respectively), outperforming the original ProxylessNAS by as much as 0.53%. Compared to the state-of-the-art NAS methods, AceNAS achieves 0.38% higher accuracy than Neural Predictor under a similar budget.

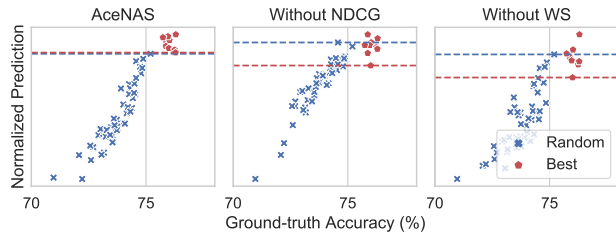


Figure 6: Qualitative ablation study of AceNAS on ProxylessNAS. The x-axis is validation accuracy (ground-truth) and y-axis is the normalized prediction score (greater is better). In the middle figure, we replace NDCG with MSE loss. In the right figure, we train the ranker without weak supervision pre-training.

Capability of finding top architectures. For a deeper understanding, we evaluate the effectiveness of NDCG and weak supervision pre-training to identify top architectures. We collect the state-of-the-art searched architectures on the ProxylessNAS search space as the best-performing architectures (first group), and randomly sample 50 architectures as the ordinary architectures (second group).

Since the accuracy of the first group (best-performing architectures) is always higher than the accuracy of the second group (randomly sampled architectures), the scores given by an ideal ranker should be linear to the ground-truth accuracy and be able to separate the two groups accordingly. As shown in Figure 6 (left), AceNAS accurately discriminate the accuracy differences of two groups.

Besides AceNAS, we train two rankers as baselines: (i) replace the LambdaRank with the MSE loss (Figure 6 (middle)), and (ii) train the ranker without pre-training (Figure 6 (right)). The results show that neither of the two baselines can separate the two groups of architectures by the prediction scores. Figure 6 (middle) indicates that, without LambdaRank, the ranker performs well as a whole (score is basically linear to ground-truth accuracy), but fails to distinguish best-performing architectures. Figure 6 (right) shows that pre-training also plays an important role. Without weak supervision pre-training, the prediction scores do not well converge to a line proportional to the accuracy.

6 Conclusion

This paper proves theoretically and empirically that NDCG is a better metric for NAS performance rankers. We then introduce AceNAS, which directly optimizes NDCG and incorporates weak supervision of weight sharing. Extensive experiments under various settings show its effectiveness.

Our study demonstrates the possibility that techniques of LTR in IR community can be applied to the NAS problem, if the discrepancies are addressed carefully. We hope our work will broaden the horizon of future NAS research.

References

- Anonymous. NAS-bench-suite: NAS evaluation is (now) surprisingly easy. In *Submitted to The Tenth International Conference on Learning Representations, 2022*. URL <https://openreview.net/forum?id=0DLwqQLmqV>. under review.
- Baker, B., Gupta, O., Raskar, R., and Naik, N. Accelerating neural architecture search using performance prediction. *arXiv preprint arXiv:1705.10823*, 2017.
- Bender, G., Kindermans, P.-J., Zoph, B., Vasudevan, V., and Le, Q. Understanding and simplifying one-shot architecture search. volume 80 of *Proceedings of Machine Learning Research*, pp. 550–559, Stockholmsmässan, Stockholm Sweden, 10–15 Jul 2018. PMLR. URL <http://proceedings.mlr.press/v80/bender18a.html>.
- Bender, G., Liu, H., Chen, B., Chu, G., Cheng, S., Kindermans, P.-J., and Le, Q. V. Can weight sharing outperform random architecture search? an investigation with tunas. In *Proceedings of the IEEE/CVF Conference on Computer Vision and Pattern Recognition*, pp. 14323–14332, 2020.
- Burges, C., Shaked, T., Renshaw, E., Lazier, A., Deeds, M., Hamilton, N., and Hullender, G. Learning to rank using gradient descent. In *Proceedings of the 22nd international conference on Machine learning*, pp. 89–96, 2005.
- Burges, C. J., Ragno, R., and Le, Q. V. Learning to rank with nonsmooth cost functions. In *Advances in neural information processing systems*, pp. 193–200, 2007.
- Cai, H., Gan, C., Wang, T., Zhang, Z., and Han, S. Once-for-all: Train one network and specialize it for efficient deployment. *arXiv preprint arXiv:1908.09791*, 2019a.
- Cai, H., Zhu, L., and Han, S. Proxylessnas: Direct neural architecture search on target task and hardware, 2019b.
- Chau, T., Dudziak, Ł., Abdelfattah, M. S., Lee, R., Kim, H., and Lane, N. D. Brp-nas: Prediction-based nas using gens. *arXiv preprint arXiv:2007.08668*, 2020.
- Cooper, W. S., Gey, F. C., and Dabney, D. P. Probabilistic retrieval based on staged logistic regression. In *Proceedings of the 15th annual international ACM SIGIR conference on Research and development in information retrieval*, pp. 198–210, 1992.
- Cramer, K. and Singer, Y. Pranking with ranking. *Advances in neural information processing systems*, 14:641–647, 2001.
- Dai, X., Zhang, P., Wu, B., Yin, H., Sun, F., Wang, Y., Dukhan, M., Hu, Y., Wu, Y., Jia, Y., Vajda, P., Uyttendaele, M., and Jha, N. K. Chamnet: Towards efficient network design through platform-aware model adaptation, 2018.
- Dai, X., Wan, A., Zhang, P., Wu, B., He, Z., Wei, Z., Chen, K., Tian, Y., Yu, M., Vajda, P., and Gonzalez, J. E. Fb-netv3: Joint architecture-recipe search using neural acquisition function, 2020.
- Dong, X. and Yang, Y. Nas-bench-201: Extending the scope of reproducible neural architecture search, 2020.
- Elsken, T., Metzen, J. H., and Hutter, F. Neural architecture search: A survey, 2018.
- Falkner, S., Klein, A., and Hutter, F. Bohb: Robust and efficient hyperparameter optimization at scale. *arXiv preprint arXiv:1807.01774*, 2018.
- Gienapp, L., Fröbe, M., Hagen, M., and Potthast, M. The impact of negative relevance judgments on ndcg. In *Proceedings of the 29th ACM International Conference on Information & Knowledge Management*, pp. 2037–2040, 2020.
- Guo, Z., Zhang, X., Mu, H., Heng, W., Liu, Z., Wei, Y., and Sun, J. Single path one-shot neural architecture search with uniform sampling, 2020.
- haowei01. pytorch-examples. <https://github.com/haowei01/pytorch-examples>, 2020.
- Howard, A., Sandler, M., Chu, G., Chen, L.-C., Chen, B., Tan, M., Wang, W., Zhu, Y., Pang, R., Vasudevan, V., Le, Q. V., and Adam, H. Searching for mobilenetv3, 2019.
- Järvelin, K. and Kekäläinen, J. Cumulated gain-based evaluation of ir techniques. *ACM Transactions on Information Systems (TOIS)*, 20(4):422–446, 2002.
- Kipf, T. N. and Welling, M. Semi-supervised classification with graph convolutional networks. *arXiv preprint arXiv:1609.02907*, 2016.
- Li, L. and Talwalkar, A. Random search and reproducibility for neural architecture search, 2019.
- Liu, H., Simonyan, K., and Yang, Y. Darts: Differentiable architecture search. *arXiv preprint arXiv:1806.09055*, 2018.
- Liu, T.-Y. *Learning to rank for information retrieval*. Springer Science & Business Media, 2011.
- Luo, R., Tan, X., Wang, R., Qin, T., Chen, E., and Liu, T.-Y. Neural architecture search with gbdt. *arXiv preprint arXiv:2007.04785*, 2020a.

- Luo, R., Tan, X., Wang, R., Qin, T., Chen, E., and Liu, T.-Y. Semi-supervised neural architecture search, 2020b.
- Mellor, J., Turner, J., Storkey, A., and Crowley, E. J. Neural architecture search without training, 2020.
- Niu, S., Wu, J., Zhang, Y., Guo, Y., Zhao, P., Huang, J., and Tan, M. Disturbance-immune weight sharing for neural architecture search, 2020.
- Peng, C., Xiao, T., Li, Z., Jiang, Y., Zhang, X., Jia, K., Yu, G., and Sun, J. Megdet: A large mini-batch object detector. In *Proceedings of the IEEE Conference on Computer Vision and Pattern Recognition (CVPR)*, June 2018.
- Pham, H., Guan, M. Y., Zoph, B., Le, Q. V., and Dean, J. Efficient neural architecture search via parameter sharing. *arXiv preprint arXiv:1802.03268*, 2018.
- Pourchot, A., Ducarouge, A., and Sigaud, O. To share or not to share: A comprehensive appraisal of weight-sharing, 2020.
- Radosavovic, I., Johnson, J., Xie, S., Lo, W.-Y., and Dollár, P. On network design spaces for visual recognition, 2019.
- Real, E., Aggarwal, A., Huang, Y., and Le, Q. V. Regularized evolution for image classifier architecture search, 2019.
- Rezaei, S. S. C., Han, F. X., Niu, D., Salameh, M., Mills, K., Lian, S., Lu, W., and Jui, S. Generative adversarial neural architecture search. *arXiv preprint arXiv:2105.09356*, 2021.
- Shi, H., Pi, R., Xu, H., Li, Z., Kwok, J. T., and Zhang, T. Bridging the gap between sample-based and one-shot neural architecture search with bonas, 2020.
- So, D. R., Liang, C., and Le, Q. V. The evolved transformer. *arXiv preprint arXiv:1901.11117*, 2019.
- Stamoulis, D., Ding, R., Wang, D., Lymberopoulos, D., Priyantha, B., Liu, J., and Marculescu, D. Single-path nas: Designing hardware-efficient convnets in less than 4 hours, 2019.
- Tan, M. and Le, Q. V. Efficientnet: Rethinking model scaling for convolutional neural networks, 2020.
- Tan, M., Chen, B., Pang, R., Vasudevan, V., Sandler, M., Howard, A., and Le, Q. V. Mnasnet: Platform-aware neural architecture search for mobile. In *Proceedings of the IEEE Conference on Computer Vision and Pattern Recognition*, pp. 2820–2828, 2019.
- Tsai, M.-F., Liu, T.-Y., Qin, T., Chen, H.-H., and Ma, W.-Y. Frank: a ranking method with fidelity loss. In *Proceedings of the 30th annual international ACM SIGIR conference on Research and development in information retrieval*, pp. 383–390, 2007.
- Wen, W., Liu, H., Chen, Y., Li, H., Bender, G., and Kindermans, P.-J. Neural predictor for neural architecture search. In *European Conference on Computer Vision*, pp. 660–676. Springer, 2020.
- White, C., Zela, A., Ru, B., Liu, Y., and Hutter, F. How powerful are performance predictors in neural architecture search?, 2021.
- Wu, B., Dai, X., Zhang, P., Wang, Y., Sun, F., Wu, Y., Tian, Y., Vajda, P., Jia, Y., and Keutzer, K. Fbnet: Hardware-aware efficient convnet design via differentiable neural architecture search. In *Proceedings of the IEEE/CVF Conference on Computer Vision and Pattern Recognition*, pp. 10734–10742, 2019.
- Xu, Y., Wang, Y., Han, K., Tang, Y., Jui, S., Xu, C., and Xu, C. Renas:relativistic evaluation of neural architecture search, 2021.
- Yan, S., Zheng, Y., Ao, W., Zeng, X., and Zhang, M. Does unsupervised architecture representation learning help neural architecture search?, 2020.
- Ying, C., Klein, A., Christiansen, E., Real, E., Murphy, K., and Hutter, F. Nas-bench-101: Towards reproducible neural architecture search. In *International Conference on Machine Learning*, pp. 7105–7114, 2019.
- Yu, K., Sciuto, C., Jaggi, M., Musat, C., and Salzmann, M. Evaluating the search phase of neural architecture search, 2019.
- Yu, K., Ranftl, R., and Salzmann, M. How to train your super-net: An analysis of training heuristics in weight-sharing nas, 2020.
- Zhang, H., Dana, K., Shi, J., Zhang, Z., Wang, X., Tyagi, A., and Agrawal, A. Context encoding for semantic segmentation, 2018a.
- Zhang, M., Cui, Z., Neumann, M., and Chen, Y. An end-to-end deep learning architecture for graph classification. In *Thirty-Second AAAI Conference on Artificial Intelligence*, 2018b.
- Zhang, Q., Han, Z., Yang, F., Zhang, Y., Liu, Z., Yang, M., and Zhou, L. Retiarri: A deep learning exploratory-training framework. In *14th {USENIX} Symposium on Operating Systems Design and Implementation ({OSDI} 20)*, pp. 919–936, 2020a.
- Zhang, Y., Lin, Z., Jiang, J., Zhang, Q., Wang, Y., Xue, H., Zhang, C., and Yang, Y. Deeper insights into weight sharing in neural architecture search, 2020b.

- Zhang, Y., Zhang, Q., and Yang, Y. How does supernet help in neural architecture search?, 2020c.
- Zhang, Y., Zhang, Q., and Yang, Y. How does supernet help in neural architecture search? In *Proceedings of the International Conference on Machine Learning*, pp. 12707–12718. PMLR, 2021.
- Zhao, Y., Wang, L., Tian, Y., Fonseca, R., and Guo, T. Few-shot neural architecture search. In *International Conference on Machine Learning*, pp. 1100–1110. PMLR, 2021.
- Zoph, B. and Le, Q. V. Neural architecture search with reinforcement learning. *arXiv preprint arXiv:1611.01578*, 2016.

A Definitions of notations

We list out the definitions of notations used throughout the paper in Table A.1.

Table A.1: The definitions of notations used through the paper.

\mathcal{A}	Search space
α	An architecture/model in the search space
n	Number of architectures to rank
k	Number of architectures selected to be fully trained and evaluated
acc	Accuracy of architecture
r	Relevance score of architecture (proportional to accuracy)
f	Ranker (ranking function)
f_ω	Ranker parameterized with ω
π_f	Ranked list (permutation) produced by f

B Implementation details

B.1 Experiments on NAS benchmarks

In this section, we first summarize the characteristics of 12 benchmarks we have experimented on. Then we introduce the settings used in weight-shared super-net training. Lastly, we elaborate the details to train GCN, including hyper-parameters and how to handle neural architectures with graph neural networks.

B.1.1 SEARCH SPACE

Apart from NAS-Bench-101 (Ying et al., 2019) and NAS-Bench-201 (Dong & Yang, 2020), which have been evaluated by many prior works, we leverage 8 more benchmarks from NDS (Radosavovic et al., 2019). These search spaces are more practical compared to NAS-Bench-101 and NAS-Bench-201, as they originate from SOTA NAS works (e.g., NASNet), search for more dimensions (e.g., up to 13 op types, width and depth) and hence contain even more architectures compared to commonly-used spaces in NAS literature.

Table B.1: Characteristics of search spaces in benchmarks: available datasets*, number of different cells in total, number of search dimension (SD), and number of architectures available in the benchmark. * all search spaces have CIFAR-10 data; † means it has CIFAR-100 data; ‡ means it has ImageNet data (NAS-Bench-201 has ImageNet 16-120 data).

Search space	# Cells	# SD	# Benchmarked
NAS-Bench-101	423,624	1	423,624
NAS-Bench-201 † ‡	15,625	1	15,625
DARTS ‡	(16, 777, 216) ²	3	5,000
DARTS-fixwd	(16, 777, 216) ²	3	5,000
ENAS ‡	(9, 765, 625) ²	3	4,999
ENAS-fixwd	(16, 777, 216) ²	3	5,000
PNAS ‡	(1, 073, 741, 824) ²	3	4,999
PNAS-fixwd	(1, 073, 741, 824) ²	3	4,599
Amoeba ‡	(1, 073, 741, 824) ²	3	4,983
NASNet ‡	(137, 858, 491, 849) ²	3	4,846

Throughout all our experiments, we follow the guidelines of (Ying et al., 2019) at our best efforts. Firstly, during the search phase, we **never** use the test dataset. We always compare architectures based on the validation accuracy. Only in the final stage, the selected single architecture is tested on the test dataset (see Algorithm 1). Secondly, to simulate the real-world scenario where an architecture is often trained only once, in each of our experiment, we randomly select one trial’s accuracy for each architecture, rather than use the average accuracy of 3 trials. We repeat every setting with at least 50 experiment runs, thus one architecture can have different accuracies in different runs. Although following these settings result in performance drop for most cases, we believe such evaluation is more realistic and we encourage followed-up works to stick to these settings.

B.1.2 WEIGHT SHARING

In the weight sharing phase of AceNAS, we use RandomNAS (*i.e.*, single-path random sampling) (Li & Talwalkar, 2019; Guo et al., 2020) to train a super-net before each search process starts. We follow (Pham et al., 2018; Guo et al., 2020; Stamoulis et al., 2019; Cai et al., 2019a) for handling the dynamic channels and depths during super-net training in NAS-Bench-101 and NDS. On evaluation, 4k architectures are evaluated for each super-net. We calculate the batch normalization statistics on the fly. We run our training on a single Nvidia Tesla V100 with 16GB memory.

We list important hyper-parameters used in super-net training in Table B.2.

Table B.2: Important hyper-parameters used in super-net training. *: In search spaces provided by NDS (Radosavovic et al., 2019), we set batch size to 128 due to limited GPU memory.

Batch size	192*
Number of epochs	600
Optimizer	SGD
Initial learning rate	0.05
Ending learning rate	0
Learning rate schedule	Cosine decay
Weight decay	0.0001
Gradient clip	5
Evaluate batch size	512

In introduction, Section 5.2.2 and Appendix E.5, several other weight-sharing approaches have been implemented. Those implementations follow one-shot algorithms provided by Microsoft NNI (Zhang et al., 2020a).

B.1.3 NDCG

As mentioned in Section 3, accuracy values are usually distributed in a large range and the distribution can be skewed. They can not be directly used as relevance scores to calculate NDCG. Therefore, we first normalize the accuracy values to a smaller range after ignoring outliers. Note that the outliers are only ignored when calculating lower and upper bound, but still taken into account in ranker training. In our experiments, we compute the 20%-quantile² of the original distribution obtained from training data (*i.e.*, architecture-accuracy pairs) as lower bound, and directly use the maximum accuracy in the training data as upper bound. This is supported by the empirical observation made by (Anonymous, 2022) (Figure 2), that, the performances of worst quarter architectures scatter in a broader range. The values in this range are then linearly mapped to $[0, S]$ to get relevance scores ($S = 20$ in experiments). Such recipe is always followed, even if the training data is lacking (only got a few architecture-accuracy pairs). Formally,

$$r_i = S \cdot \max\left(\frac{\text{acc}_i - \text{Quantile}(\{\text{acc}_i\}, 0.2)}{\max_{1 \leq i \leq n} \text{acc}_i - \text{Quantile}(\{\text{acc}_i\}, 0.2)}, 0\right) \quad (8)$$

where acc_i refers to the accuracy of the i -th architecture, and r_i refers to the computed relevance score that is used in NDCG. The outer $\max(\cdot, 0)$ is because NDCG cannot take negative relevance scores, as pointed out by (Gienapp et al., 2020).

Figure B.1 shows an illustration of this process on NAS-Bench-201. In this example, around 80% of the accuracy values are located between 60% and 70%, while the other 20% accuracy values span from 0 to 60% (we call them outliers). We clip the accuracy to a narrower range to distinguish the top 80% architectures.

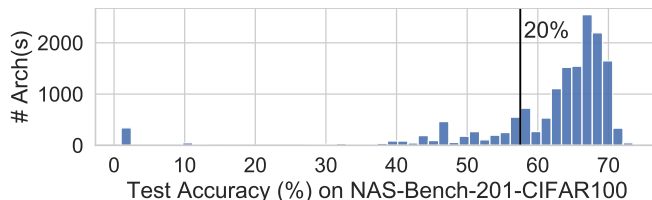


Figure B.1: Test accuracy distribution in NAS-Bench-201.

In Appendix E.1.2, we further compare different choices of S and different approaches to compute the lower bound.

²We use the implementation of `numpy.quantile`.

B.1.4 GCN

A crucial step to build a performance ranker for neural architectures, is to get an appropriate embedding of architectures, *i.e.*, converting dynamically constructed graphs with different depth and width into a fixed-length vector. Graph Convolutional Network (GCN) (Kipf & Welling, 2016) is a natural fit for generating the embedding due to its advantage in dealing with graph-structured data, thus it has been adopted in recent works (Chau et al., 2020; Wen et al., 2020). We also use GCN for the embedding. Specifically we choose Deep Graph Convolutional Neural Network (DGCNN) (Zhang et al., 2018b) which performs well in our model. It has four directed graph convolution layers followed by sort-pooling (Zhang et al., 2018b) and 1D convolution as shown in Figure B.2.

Following (Wen et al., 2020), we encode one type of cell into a directed graph. The type of operator is encoded into a one-hot tensor that is treated as node attributes, and the connections between operators are encoded as edges. Some other pseudo-nodes are necessary to make the graph connected, for example the nodes that are labeled as add/input/output/concatenate. In search spaces provided by NDS, the neural networks search for multiple different types of cells and a series of architecture hyper-parameters (*e.g.*, number of cells stacked, channel size multiplier). The graphs are then fed into GCN and the embedded features are concatenated with hyper-parameter features.

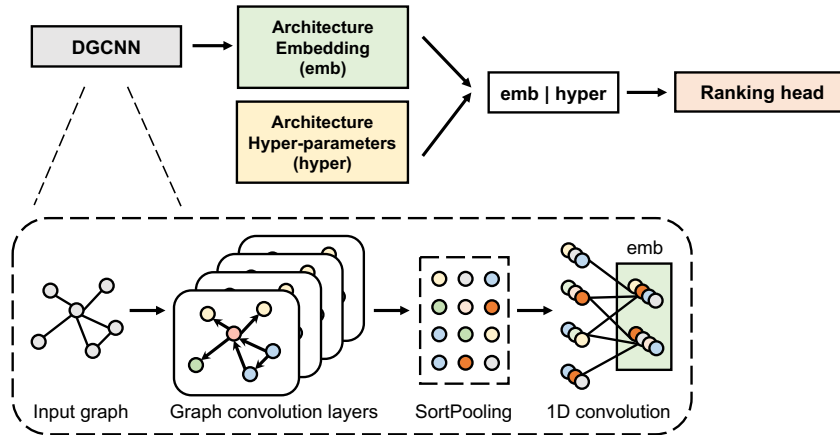


Figure B.2: Architecture of our performance ranker.

Another component in the performance ranker is ranking head. Our ranking head is a Multi-layer Perceptron, which in our case are two fully-connected layers with ReLU and dropout in between. It predicts ranking score s_i^* for an architecture α_i by taking α_i 's embedding from DGCNN and corresponding hyper-parameters. With the ranking score, we use Equation (5) and Equation (6) to optimize the ranker. σ in Equation (6) is set to 1.

The ranker is trained using *iterative sampling* which has been widely used in AutoML algorithms (*e.g.*, BOHB (Falkner et al., 2018) and BRP-NAS (Chau et al., 2020)). We split the training process into multiple rounds. In each round, we train n architectures and get n architecture-accuracy pairs, which are used to train the ranker. Then, the ranker is used to sample architectures for the next round. To balance exploration and exploitation, in each round, we sample $\varepsilon \cdot n$ best architectures with our ranker, while the other $(1 - \varepsilon) \cdot n$ are sampled randomly. ε is set of 0.5 in our experiments.

To empower our ranker with knowledge from super-net, we replace ranking head in the ranker (Figure B.2) with a WS-accuracy head, a FLOPs head, and a parameters head, which are three two-layer MLPs to predict weight sharing accuracy, FLOPs and number of parameters respectively. The whole ranker is then pretrained to minimize the loss defined in Equation (7). Empirically we find that the training is not sensitive to λ_1 and λ_2 , after we normalize the ground truth labels by subtracting mean and dividing by standard deviation. Therefore we simply set $\lambda_1 = \lambda_2 = 1$.

We use PyTorch³ for GCN implementation. We list important hyper-parameters of ranker training in AceNAS in Table B.3. For BRP-NAS (Chau et al., 2020) and Neural predictor (Wen et al., 2020), we follow the hyper-parameters used in their paper.

³We refer to (haowei01, 2020) when implementing LTR algorithms.

Table B.3: Important hyper-parameters used in ranker training. In pre-training stage, we use the same hyper-parameters, except initial learning rate = 0.001, weight decay = 10^{-5} and early stop is disabled.

Hidden units	128
Batch size	20
Number of epochs	300
Optimizer	Adam
Initial learning rate	0.005
Ending learning rate	0
Learning rate schedule	Cosine decay
Weight decay	0.0005
Early stop patience	50

B.2 Experiments on ProxylessNAS

To run experiment on ProxylessNAS, we first train a super-net with single-path random sampling (Li & Talwalkar, 2019; Guo et al., 2020). The hyper-parameters used are slightly different from those listed in Table B.3. We list them in Table B.4. We followed the implementation in (Bender et al., 2020) to sample skip connection at 0.5 probability, although we did not apply other tricks, *e.g.*, merging convolution kernels. After super-net training is done, we sampled 10000 architectures, where half of them satisfy the latency constraint (83 – 85ms) and the other half are randomly sampled from the distribution used in super-net training phase.

Table B.4: Important hyper-parameters used in super-net training of ProxylessNAS. *: We split the 2048 batch size into 16 GPUs and in each mini-batch every GPU samples architectures independently.

Batch size	2048 *
Number of epochs	360
Warm-up epochs	5
Optimizer	SGD
Initial learning rate	0.48
Ending learning rate	0
Learning rate schedule	Cosine decay
Weight decay	0.00005
Accelerator	16 GPUs

To train GCN, we used hyper-parameters identical to Table B.3, except that initial learning rate is decreased to 0.001.

To train the searched architecture (both in the validation setting and test setting), we followed the settings proposed by (Bender et al., 2020). Concretely, during the search process, each architecture is trained for 90 epochs. The final selected architectures are retrained with a longer schedule (360 epochs) with dropout rate 0.15 before the final fully-connected layer. We re-implement it with PyTorch as the original implementation supports TPU only. To align the batch size (4096) with the original setting, we use 16 V100 GPU so that each GPU takes a mini-batch of 256 samples. Ideally, Sync-BN (Peng et al., 2018; Zhang et al., 2018a) should be applied to synchronize batch normalization on all GPUs, however, we find that it harms the training speed by about 50%. To balance training speed and performance, we used Distribute-BN that synchronizes running statistics of batch normalization at the end of each epoch.

Training a single architecture with 90 epochs take around 5 hours on 16 V100 GPUs, which is around 80 GPU hours. It sums up to 780 GPU days to train all 234 architectures in the search process. To speedup this process, we leverage the metrics of randomly selected architectures from (Bender et al., 2020) when AceNAS requests for a new random architecture to be run. This saves the training cost of 140 architectures and thus reduces the total cost to 313 GPU days.

C Pseudo-code of AceNAS

In Algorithm 1, we present the pseudo-code of AceNAS.

Algorithm 1 AceNAS

Input: Search space \mathcal{A} , budget for each round n , budget after training k , number of rounds R , exploration-exploitation factor ε . Dataset $\mathcal{D}_{\text{train}}$, \mathcal{D}_{val} and $\mathcal{D}_{\text{test}}$.

Output: The ranker f_ω , the best architecture α^\dagger , the best test accuracy acc^\dagger .

▷ *Pre-training*

Build a weight sharing super-net S based on \mathcal{A} .

while not converged **do**

 Random sample one sub-net α from super-net.

 Optimize weights corresponding to α and update in S .

end while

Sample sufficient architectures from \mathcal{A} and evaluate accuracy, FLOPs and number of parameters on S

Optimize f_ω to minimize $\mathcal{L}_{mse}(\text{acc}_i, \text{acc}_i^*) + \lambda_1 \cdot \mathcal{L}_{mse}(\text{flops}_i, \text{flops}_i^*) + \lambda_2 \cdot \mathcal{L}_{mse}(\text{params}_i, \text{params}_i^*)$.

▷ *Fine-tuning*

Initialize sampled architectures $A = \emptyset$

for $i = 1, \dots, R$ **do**

 ▷ *When the search space is very large, the following step can be solved with evolution.*

$A' \leftarrow$ best $\varepsilon \cdot n$ architectures predicted by f_ω and $(1 - \varepsilon) \cdot n$ random architectures.

$A \leftarrow A \cup \{(\alpha, \text{TRAINANDEVAL}(\alpha, \mathcal{D}_{\text{train}}, \mathcal{D}_{\text{val}}) \mid \alpha \in A'\}$. ▷ *This is the most costly step.*

 Fine-tune ranker f_ω on A with LambdaRank.

end for

$A' \leftarrow$ top- k architectures predicted by f_ω .

$A \leftarrow A \cup \{(\alpha, \text{TRAINANDEVAL}(\alpha, \mathcal{D}_{\text{train}}, \mathcal{D}_{\text{val}}) \mid \alpha \in A'\}$.

$\alpha^\dagger \leftarrow$ architecture with best validation accuracy on A .

$\text{acc}^\dagger \leftarrow \text{TRAINANDEVAL}(\alpha, \mathcal{D}_{\text{train}}, \mathcal{D}_{\text{test}})$

D Proof of theorems in Section 3

D.1 Proof of Theorem 3.2

Proof. According to the assumption, we have,

$$\sum_{i=1}^n \frac{1}{\log_2(i+1)} (2^{r_{\pi_f(i)}} - 1) \geq \nu \left(\sum_{i=1}^n \frac{1}{\log_2(i+1)} (2^{r_i} - 1) \right) \quad (9)$$

Let $r^* = \max_{1 \leq i \leq k} r_{\pi_f(i)}$. Since $r_1 \geq r_2 \geq \dots \geq r_n$ and $r^* \geq r_{\pi_f(i)}$ for $1 \leq i \leq k$, we get the following inequality:

$$\sum_{i=1}^k \frac{1}{\log_2(i+1)} (2^{r^*} - 1) + \sum_{i=k+1}^n \frac{1}{\log_2(i+1)} (2^{r_{i-k}} - 1) \geq \sum_{i=1}^n \frac{1}{\log_2(i+1)} (2^{r_{\pi_f(i)}} - 1) \geq \nu \left(\sum_{i=1}^n \frac{1}{\log_2(i+1)} (2^{r_i} - 1) \right) \quad (10)$$

Expand the inequality, we get,

$$2^{r^*} \left(\sum_{i=1}^k \frac{1}{\log_2(i+1)} \right) \geq \sum_{i=1}^{n-k} 2^{r_i} \left(\frac{\nu}{\log_2(i+1)} - \frac{1}{\log_2(i+k+1)} \right) + \sum_{i=n-k+1}^n 2^{r_i} \left(\frac{\nu}{\log_2(i+1)} \right) + (1-\nu) \sum_{i=1}^n \frac{1}{\log_2(i+1)} \quad (11)$$

Recall that c_i is defined to be a sequence of length n :

$$c_i^{(\nu, k)} = \begin{cases} \frac{1}{\log_2(i+1)} - \frac{1}{\nu \log_2(i+k+1)} & \text{if } 1 \leq i \leq n-k \\ \frac{1}{\log_2(i+1)} & \text{if } n-k+1 \leq i \leq n \end{cases} \quad (12)$$

By assumption, it is easy to verify that $c_i^{(\nu, k)} > 0$ for $1 \leq i \leq n$.

Then Equation (11) can be rewritten as:

$$2^{r^*} \left(\sum_{i=1}^k \frac{1}{\log_2(i+1)} \right) \geq \nu \sum_{i=1}^n 2^{r_i} c_i^{(\nu,k)} + (1-\nu) \sum_{i=1}^n \frac{1}{\log_2(i+1)} \quad (13)$$

Take log on both sides:

$$\begin{aligned} r^* &\geq \log_2 \left(\nu \sum_{i=1}^n 2^{r_i} c_i^{(\nu,k)} + (1-\nu) \sum_{i=1}^n \frac{1}{\log_2(i+1)} \right) - \log_2 \left(\sum_{i=1}^k \frac{1}{\log_2(i+1)} \right) \\ &\geq \nu \log_2 \left(\sum_{i=1}^n 2^{r_i} c_i^{(\nu,k)} \right) + (1-\nu) \log_2 \left(\sum_{i=1}^n \frac{1}{\log_2(i+1)} \right) - \log_2 \left(\sum_{i=1}^k \frac{1}{\log_2(i+1)} \right) \end{aligned} \quad (14)$$

$$\geq \nu \left(\frac{\sum_{i=1}^n r_i c_i^{(\nu,k)}}{\sum_{i=1}^n c_i^{(\nu,k)}} + \log_2 \left(\sum_{i=1}^n c_i^{(\nu,k)} \right) \right) + (1-\nu) \log_2 \left(\sum_{i=1}^n \frac{1}{\log_2(i+1)} \right) - \log_2 \left(\sum_{i=1}^k \frac{1}{\log_2(i+1)} \right) \quad (15)$$

$$\begin{aligned} &= \nu \left(\frac{\sum_{i=1}^n r_i c_i^{(\nu,k)}}{\sum_{i=1}^n c_i^{(\nu,k)}} \right) + \nu \log_2 \frac{L(k) + (1-\frac{1}{\nu})(L(n) - L(k))}{L(n)} + \log_2 \frac{L(n)}{L(k)} \\ &= \nu \left(\frac{\sum_{i=1}^n r_i c_i^{(\nu,k)}}{\sum_{i=1}^n c_i^{(\nu,k)}} \right) + \log_2 \left(1 - \frac{L(n) - L(k)}{\nu \cdot L(n)} \right)^\nu + \log_2 \frac{L(n)}{L(k)} \end{aligned} \quad (16)$$

Here Equation (14) and Equation (15) is obtained by using Jensen's inequality twice, and we use $L(n)$ to denote the prefix sum of $\frac{1}{\log_2(i+1)}$, i.e., $L(n) = \sum_{i=1}^n \frac{1}{\log_2(i+1)}$. On the other hand, since $k \gg (n+1) - (n+1)^\nu$, $\nu > \frac{\log_2(n-k+1)}{\log_2(n+1)}$,

$$\frac{L(n) - L(k)}{\nu \cdot L(n)} < \frac{\log_2(n+1)(L(n) - L(k))}{\log_2(n-k+1)L(n)} \quad (17)$$

$$\leq \frac{\ln(n+1)(\text{Li}(n+1) - \text{Li}(k+1))}{\ln(n-k+1)\text{Li}(n+2)} \quad (18)$$

$$\leq 1 \quad (19)$$

where $\text{Li}(x) = \int_2^x \frac{dt}{\ln t} = \text{li}(x) - \text{li}(2)$, is the "offset logarithmic integral". Equation (18) is by using left/right Riemann sums to bound the sum of $\frac{1}{\log_2(i+1)}$. See Lemma D.2 for the proof of the last step.

Combining Equation (16) and Equation (19), along with Bernoulli's inequality, we have,

$$\begin{aligned} r^* &\geq \nu \left(\frac{\sum_{i=1}^n r_i c_i^{(\nu,k)}}{\sum_{i=1}^n c_i^{(\nu,k)}} \right) + \log_2 \left(1 - \nu \frac{L(n) - L(k)}{\nu \cdot L(n)} \right) + \log_2 \frac{L(n)}{L(k)} \\ &= \nu \left(\frac{\sum_{i=1}^n r_i c_i^{(\nu,k)}}{\sum_{i=1}^n c_i^{(\nu,k)}} \right) \end{aligned} \quad (20)$$

□

A followed corollary of Theorem 3.2 is,

Corollary D.1. *If $NDCG(f; \mathbf{a}, \mathbf{r}) \geq \nu$ and $k > (n+1) - (n+1)^\nu$, $TopK(f; \mathbf{a}, \mathbf{r}, k) \geq h(\nu)$, where $h(\nu)$ is a increasing function of ν .*

Proof. We let,

$$h(\nu) = \nu \left(\frac{\sum_{i=1}^n r_i c_i}{\sum_{i=1}^n c_i} \right) \quad (21)$$

We note that $(\sum_{i=1}^n r_i c_i) / (\sum_{i=1}^n c_i)$ is a c_i -weighted average of r_i . For $i \leq n - k$, c_i is increasing when ν increases. Furthermore, the increment is larger when i is smaller, where $\frac{1}{\log_2(i+k+1)}$ is larger. Hence, the weighted average leans to larger r_i 's as ν increases.

We conclude $h(\nu)$ is a monotonically increasing function of ν . \square

Lemma D.2. Let $\rho(n, k) := \frac{\ln(n+1)(\text{Li}(n+1) - \text{Li}(k+1))}{\ln(n-k+1)\text{Li}(n+2)}$. $\rho(n, k) \leq 1$ for all integers $n \geq k \geq 1$.

Proof. Firstly, we show that $\rho(n, 1) \leq 1$.

We define $h(n)$ to be,

$$h(n) = \ln\left(\frac{n+1}{n}\right) \text{Li}(n+1) - \frac{\ln(n)}{\ln(n+2)} \quad (22)$$

Since,

$$\frac{\delta h(n)}{\delta n} = \log_{(1+n)}\left(1 + \frac{1}{n}\right) - \frac{\ln\left(\frac{n^{1/(n+2)}}{(n+2)^{1/n}}\right)}{\ln^2(n+2)} - \frac{\text{Li}(n+1)}{n(n+1)} < 0 \quad (23)$$

$h(n)$ is a monotonically decreasing function of n .

On the other hand, we have,

$$\begin{aligned} \ln(n+1)\text{Li}(n+1) - \ln(n)\text{Li}(n+2) &< \ln(n+1)\text{Li}(n+1) - \ln(n)\left(\text{Li}(n+1) + \frac{1}{\ln(n+2)}\right) \\ &= h(n) \leq h(1) = 0 \end{aligned} \quad (24)$$

Hence,

$$\rho(n, 1) = \frac{\ln(n+1)\text{Li}(n+1)}{\ln(n)\text{Li}(n+2)} \leq 1 \quad (25)$$

Then, we show $\rho(n, k)$ is a monotonically decreasing function of k .

$$\frac{\delta \rho(n, k)}{\delta k} = \frac{\ln(n+1)(\ln(k+1)(\text{Li}(n+1) - \text{Li}(k+1)) - (n-k+1)\ln(n-k+1))}{(n+1-k)\ln(k+1)\ln^2(n+1-k)(\text{Li}(n+2))} \quad (26)$$

Obviously, the sign of Equation (27) depends on the sign of $(\ln(k+1) \cdots \ln(n-k+1))$. Let $\alpha = k+1$, $\beta = n-k+1$, so that $\alpha + \beta = n+2$, and $2 \leq \alpha \leq n+1$, $1 \leq \beta \leq n$. Then,

$$\text{sign}\left(\frac{\delta \rho(n, k)}{\delta k}\right) = \text{sign}(\ln \alpha (\text{Li}(\alpha + \beta - 1) - \text{Li}(\alpha)) - \beta \ln \beta) \quad (27)$$

Since we have,

$$\text{Li}(\alpha + \beta - 1) - \text{Li}(\alpha) = \int_{\alpha}^{\alpha + \beta - 1} \frac{dt}{\ln t} \leq \frac{\beta - 1}{\ln \alpha} \quad (28)$$

Combining Equation (27) and Equation (28), we get,

$$\text{sign}\left(\frac{\delta \rho(n, k)}{\delta k}\right) \leq \text{sign}(\beta(1 - \ln \beta) - 1) < 0 \quad (29)$$

Hence, we conclude $\rho(n, k) \leq \rho(n, 1) \leq 1$.

\square

D.2 Proof of Theorem 3.3

Proof. For a ranker f , let $\text{TopK}(f; \mathbf{a}, \mathbf{r}, k) \geq y_t$, where $1 \leq t \leq n - k + 1$. Since $\mathbb{E}[\text{NDCG}(f; \mathbf{a}, \mathbf{r})] = \frac{\mathbb{E}[\text{DCG}(f; \mathbf{a}, \mathbf{r})]}{\text{IDCG}(f; \mathbf{a}, \mathbf{r})}$, we only need to prove that, $\mathbb{E}[\text{DCG}(f; \mathbf{a}, \mathbf{r})]$ is a monotonically decreasing function of t .

Since we want to have at least one of $\pi_f(1), \pi_f(2), \dots, \pi_f(k)$ to be at most t , the total number of different π_f that satisfies such condition is,

$$C_{\text{tot}}(n, k, t) = n! - \frac{(n-t)!(n-k)!}{(n-t-k)!} \quad (30)$$

Then, we compute the number of permutations where $\pi_f(i) = j$ ($1 \leq j \leq n$), which we denote as $C(i, j; n, k, t)$. Apparently, $i = 1, 2, \dots, k$ are symmetric, *i.e.*, $C(i_1, j) = C(i_2, j)$ for $1 \leq i_1, i_2 \leq k$. The same is for $i = k + 1, k + 2, \dots, n$, $j = 1, 2, \dots, t$, and $j = t + 1, t + 2, \dots, n$. Thus, $C(i, j)$ can be divided into four cases:

$$C(i, j; n, k, t) = \begin{cases} (n-1)! & \text{if } 1 \leq i \leq k \text{ and } 1 \leq j \leq t \\ (C_{\text{tot}}(n, k, t) - t \cdot (n-1)!)/ (n-t) & \text{if } 1 \leq i \leq k \text{ and } t+1 \leq j \leq n \\ (n-1)! - \frac{(n-t)!(n-k-1)!}{(n-t-k)!} & \text{if } k+1 \leq i \leq n \text{ and } 1 \leq j \leq t \\ \left(C_{\text{tot}}(n, k, t) - t \cdot \left((n-1)! - \frac{(n-t)!(n-k-1)!}{(n-t-k)!} \right) \right) / (n-t) & \text{if } k+1 \leq i \leq n \text{ and } t+1 \leq j \leq n \end{cases} \quad (31)$$

Note that the expressions in Equation (31) can be further simplified, but we keep them in their raw forms so that readers can easily see where they come from.

On the other hand, $\mathbb{E}[\text{DCG}(f; \mathbf{a}, \mathbf{r})]$ can be evaluated as:

$$\begin{aligned} \mathbb{E}[\text{DCG}(f; \mathbf{a}, \mathbf{r})] &= \mathbb{E} \left[\sum_{i=1}^n \frac{1}{\log_2(i+1)} (2^{r_{\pi_f(i)}} - 1) \right] \\ &= \sum_{i=1}^n \frac{1}{\log_2(i+1)} [\mathbb{E}(2^{r_{\pi_f(i)}}) - 1] \\ &= \sum_{i=1}^n \frac{1}{\log_2(i+1)} \left[\sum_{j=1}^n 2^{r_j} \cdot \Pr(\pi_f(i) = j) - 1 \right] \\ &= \sum_{i=1}^n \frac{1}{\log_2(i+1)} \left[\sum_{j=1}^n 2^{r_j} \cdot \frac{C(i, j; n, k, t)}{C_{\text{tot}}(n, k, t)} - 1 \right] \end{aligned} \quad (32)$$

By substituting Equation (31) into Equation (32), we get:

$$\begin{aligned} \mathbb{E}[\text{DCG}(f; \mathbf{a}, \mathbf{r})] &= \left[\left(\sum_{i=1}^k \frac{1}{\log_2(i+1)} \right) \left(\sum_{j=1}^t 2^{r_j} \right) (n-1)! \right. \\ &\quad + \left(\sum_{i=1}^k \frac{1}{\log_2(i+1)} \right) \left(\sum_{j=t+1}^n 2^{r_j} \right) \left(\frac{n!}{n-t} - \frac{(n-t-1)!(n-k)!}{(n-t-k)!} - \frac{t \cdot (n-1)!}{n-t} \right) \\ &\quad + \left(\sum_{i=k+1}^n \frac{1}{\log_2(i+1)} \right) \left(\sum_{j=1}^t 2^{r_j} \right) \left((n-1)! - \frac{(n-t)!(n-k-1)!}{(n-t-k)!} \right) \\ &\quad + \left(\sum_{i=k+1}^n \frac{1}{\log_2(i+1)} \right) \left(\sum_{j=t+1}^n 2^{r_j} \right) \left(\frac{n!}{n-t} - \frac{(n-t-1)!(n-k)!}{(n-t-k)!} \right. \\ &\quad \left. - t \cdot \left(\frac{(n-1)!}{n-t} - \frac{(n-t-1)!(n-k-1)!}{(n-t-k)!} \right) \right) \\ &\quad \left. \right] / \left(n! - \frac{(n-t)!(n-k)!}{(n-t-k)!} \right) \end{aligned} \quad (33)$$

For notation simplicity, for the rest of this proof, we use $L(n) = \sum_{i=1}^n \frac{1}{\log_2(i+1)}$, and $R(n) = \sum_{i=1}^n 2^{r_i}$. After this, Equation (33) can be further rewritten and simplified as:

$$\begin{aligned} \mathbb{E}[\text{DCG}(f; \mathbf{a}, \mathbf{r})] &= \frac{(nR(t)L(k) + kR(n)L(n) - (nR(n) + kR(t))L(n) + tR(n)(L(n) - L(k))(n-k-1)(n-t-1)!)}{n!(n-t-k)! - (n-t)!(n-k)!} \\ &\quad + \frac{R(n)L(n)(n-1)!(n-k-t)!}{n!(n-t-k)! - (n-t)!(n-k)!} \end{aligned} \quad (34)$$

Define $\gamma(n, t, k)$ as $\binom{n}{k} / \binom{n-t}{k}$. We rewrite Equation (34) with $\gamma(n, t, k)$:

$$\begin{aligned} \mathbb{E}[\text{DCG}(f; \mathbf{a}, \mathbf{r})] &= \frac{(nR(t)L(k) + kR(n)L(n) - (nR(n) + kR(t))L(n) + tR(n)(L(n) - L(k))\gamma(n, t, k))}{(n-t)(n-k)(1 - \gamma(n, t, k))} \\ &\quad + \frac{R(n)L(n)}{n(1 - \gamma(n, t, k))} \end{aligned} \quad (35)$$

By Stirling's formula, when $n \gg k$, $\gamma(n, t, k)$ can be approximated as,

$$\gamma(n, t, k) = \binom{n}{k} / \binom{n-t}{k} = \frac{n!(n-t-k)!}{(n-t)!(n-k)!} \approx \left(\frac{n-t}{n}\right)^k \quad (36)$$

Thus, by replacing $\gamma(n, t, k)$ with Equation (36), Equation (35) becomes,

$$\mathbb{E}[\text{DCG}(f; \mathbf{a}, \mathbf{r})] = \left(\frac{R(n)L(n)}{n} + \frac{\left(\frac{n-t}{n}\right)^k (L(k)(nR(t) - tR(n)) - L(n)((n-k-t)R(n) + kR(t)))}{(n-t)(n-k)} \right) / \left(1 - \left(\frac{n-t}{n}\right)^k \right) \quad (37)$$

We then take the partial derivative of $\mathbb{E}[\text{DCG}(f; \mathbf{a}, \mathbf{r})]$ with respect to t :

$$\frac{\delta \mathbb{E}[\text{DCG}(f; \mathbf{a}, \mathbf{r})]}{\delta k} = \frac{\zeta(nL(k) - kL(n)) \left((n(\zeta - 1) + kt)R(n) + n(n-t)(1-\zeta) \frac{\delta R(t)}{\delta t} - n(\zeta + k - 1)R(t) \right)}{n(n-k)(n-t)^2 (\zeta - 1)^2} \quad (38)$$

Note that in this equation (and for the rest of this proof), we use $\zeta = \left(1 - \frac{t}{n}\right)^k$, which is implicitly an function of n, t , and k , to simplify the notation.

In Equation (38), obviously the denominator is greater than 0. $0 < \zeta < 1$. $nL(k) - kL(n) > 0$ because $L(n) \approx \text{Li}(n) \cdot \ln 2 \sim \frac{n}{\ln n}$. For the coefficient of $\frac{\delta R(t)}{\delta t}$ and $R(t)$, $n(n-t)(1-\zeta) > 0$, while $-n(\zeta + k - 1) < 0$. On the other hand, we have,

$$\frac{\delta R(t)}{\delta t} \approx 2^{r_t}, \quad \text{and} \quad (39)$$

$$R(t) = \sum_{i=1}^t 2^{r_i} \geq t2^{r_t} \quad (40)$$

Therefore,

$$\begin{aligned} \text{sign} \left(\frac{\delta \mathbb{E}[\text{DCG}(f; \mathbf{a}, \mathbf{r})]}{\delta k} \right) &= \text{sign} \left((n(\zeta - 1) + kt)R(n) + n(n-t)(1-\zeta) \frac{\delta R(t)}{\delta t} - n(\zeta + k - 1)R(t) \right) \\ &\leq \text{sign} \left((n(\zeta - 1) + kt)R(n) + n(n-t)(1-\zeta) 2^{r_t} - n(\zeta + k - 1)t2^{r_t} \right) \\ &= \text{sign} \left((R(n) - n2^{r_t})((\zeta - 1)n + kt) \right) \end{aligned} \quad (41)$$

By Bernoulli's inequality, $\zeta = \left(1 - \frac{t}{n}\right)^k \geq 1 - \frac{kt}{n}$. Hence, $(\zeta - 1)n + kt \geq 0$. Since $R(n) \leq n2^{r_t}$ by assumption, $\frac{\delta \mathbb{E}[\text{DCG}(f; \mathbf{a}, \mathbf{r})]}{\delta k} > 0$. We conclude that $\mathbb{E}[\text{DCG}(f; \mathbf{a}, \mathbf{r})]$ is a function that is monotonically decreasing to k , thus complete the proof. \square

E More experiment results

E.1 Empirical study of NDCG

E.1.1 CORRELATION BETWEEN NDCG AND ACCURACY

To answer the question whether NDCG is a good indicator, we first collect a number of rankers on each search space, which spans rankers based on weight sharing, several performance predictors, and AceNAS. We run each of them once, and measure their NDCG and top-10 test accuracy in Figure E.1. The upward trend in this figure indicates a positive correlation between NDCG and test accuracy. Notably on the spaces of NAS-Bench-201, for rankers achieving test accuracy between 70% and 75%, NDCG spans a wide range from 0.6 and 0.9, indicating that NDCG is numerically sensitive to top-performing architectures.

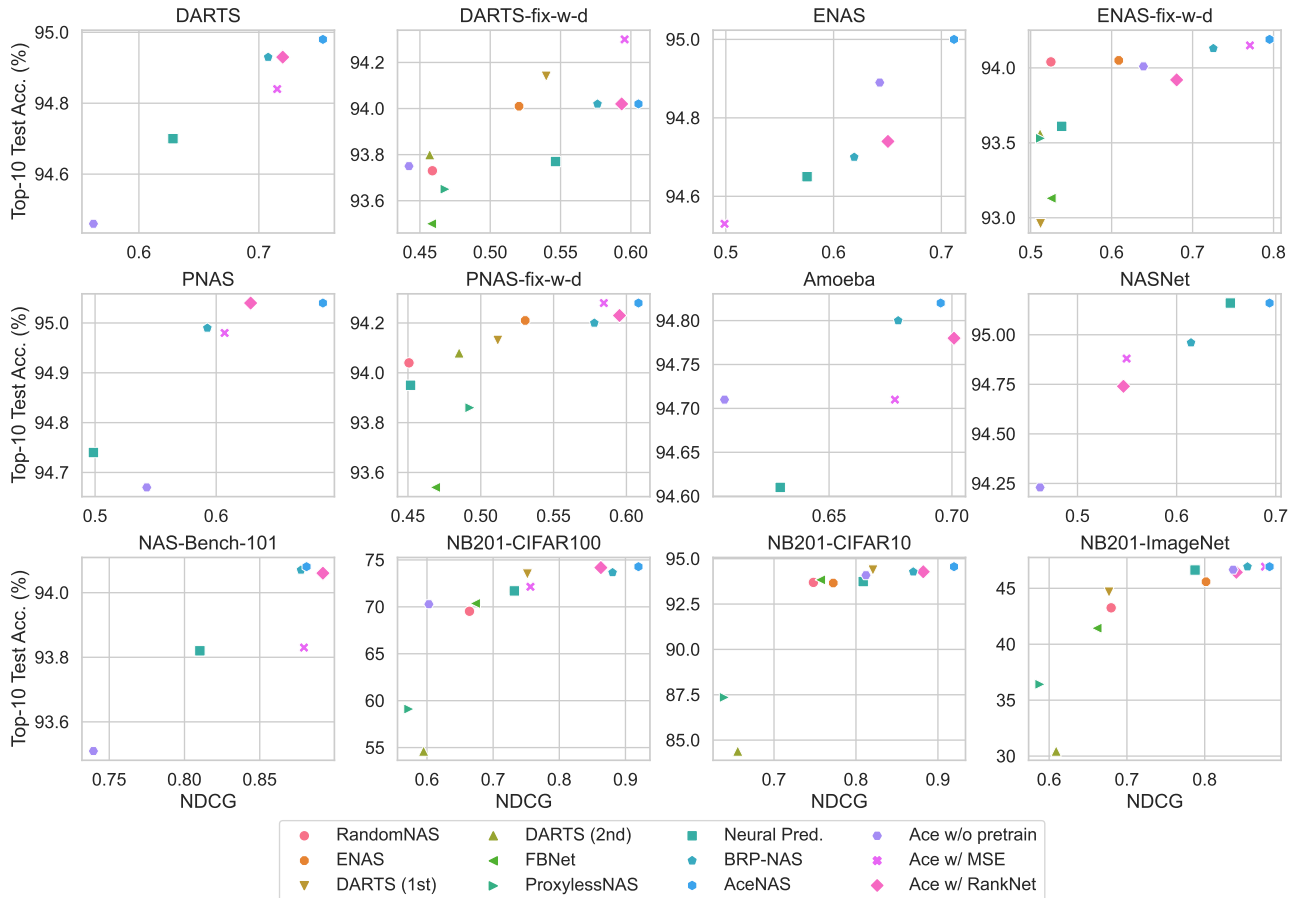


Figure E.1: Scatter-plot of NDCG vs. top-10 test accuracy of a various kind of rankers, experimented on various search spaces.

A similar scatter-plot is shown in Figure E.2, which illustrates the relationship between KdT and test accuracy. In this figure, we observe many cases where a ranker with a high KdT does not have a good test accuracy. Another interesting finding is that AceNAS’s variant (AceNAS w/ RankNet) enjoys KdT close to AceNAS on most search spaces, and sometimes it is even better, but final accuracy is relatively low. Comparing Figure E.1 with Figure E.2, we can conclude once more, that KdT is a worse metric for rankers than NDCG.

Moreover, we collect NDCG metric of all experiments and runs covered in Section 5, and show them in Figure E.3. In this figure, each point corresponds to an experiment (*i.e.*, a performance ranker trained with a specific seed and budget). In this figure, we see an upward trend which is similar to Figure E.1. When looking at points with different markers and colors, we further point out the distribution of different methods, which illustrates how AceNAS improves NDCG and accuracy simultaneously. Compared to points from Vanilla and BRP-NAS, most points from AceNAS are at the top-right corner,

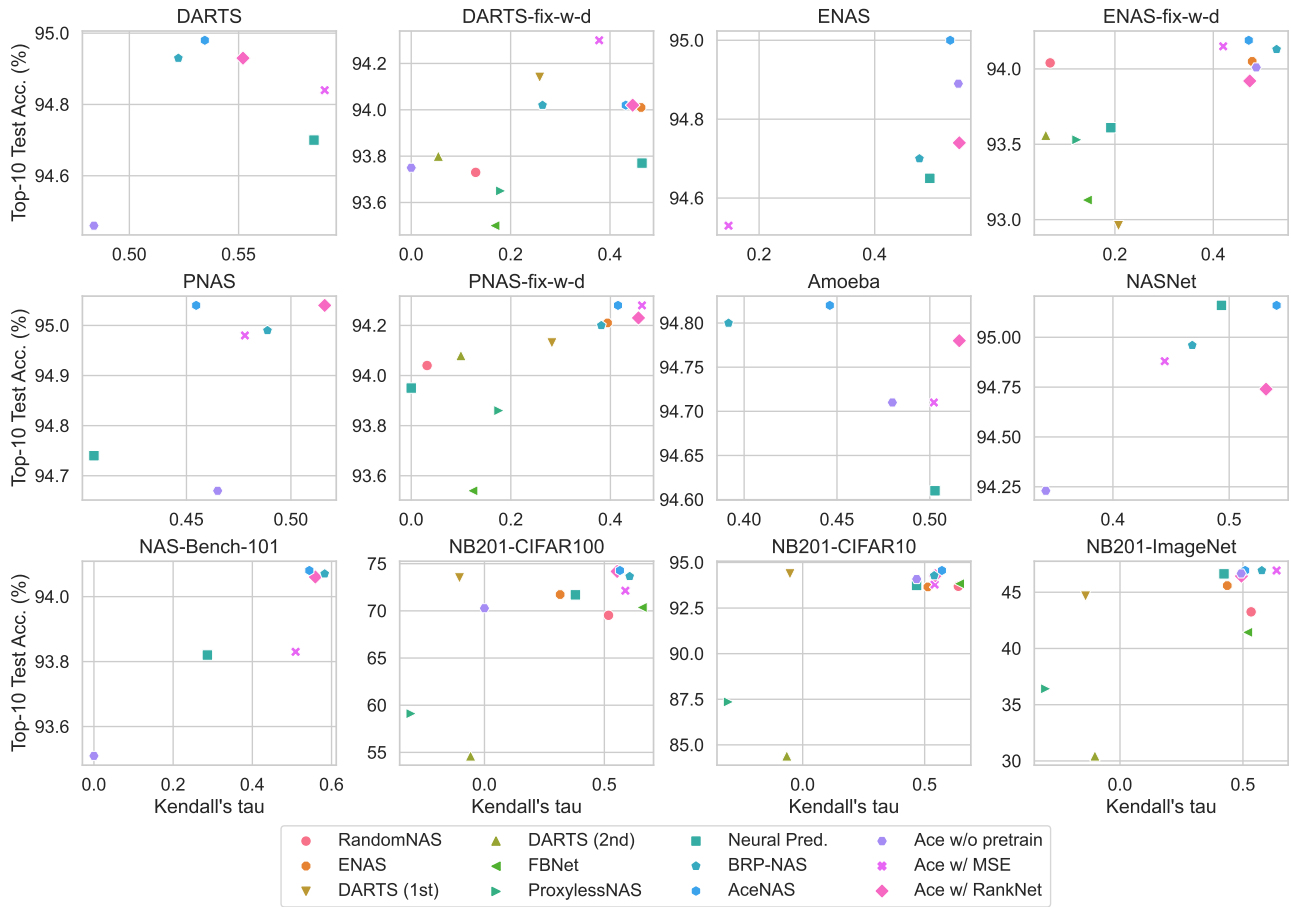


Figure E.2: Scatter-plot of KdT vs. top-10 test accuracy of a various kind of rankers, experimented on various search spaces.

meaning that they enjoy both a better NDCG and a better test accuracy at the same time.

We also calculate the pearson correlation between NDCG and test accuracy (*i.e.*, x - y correlation in Figure E.1) and we find that NDCG is well correlated with the end-to-end goal of NAS (up to ~ 0.8 correlation). This is higher than the correlation between KdT and test accuracy. The results are shown in Figure E.4.

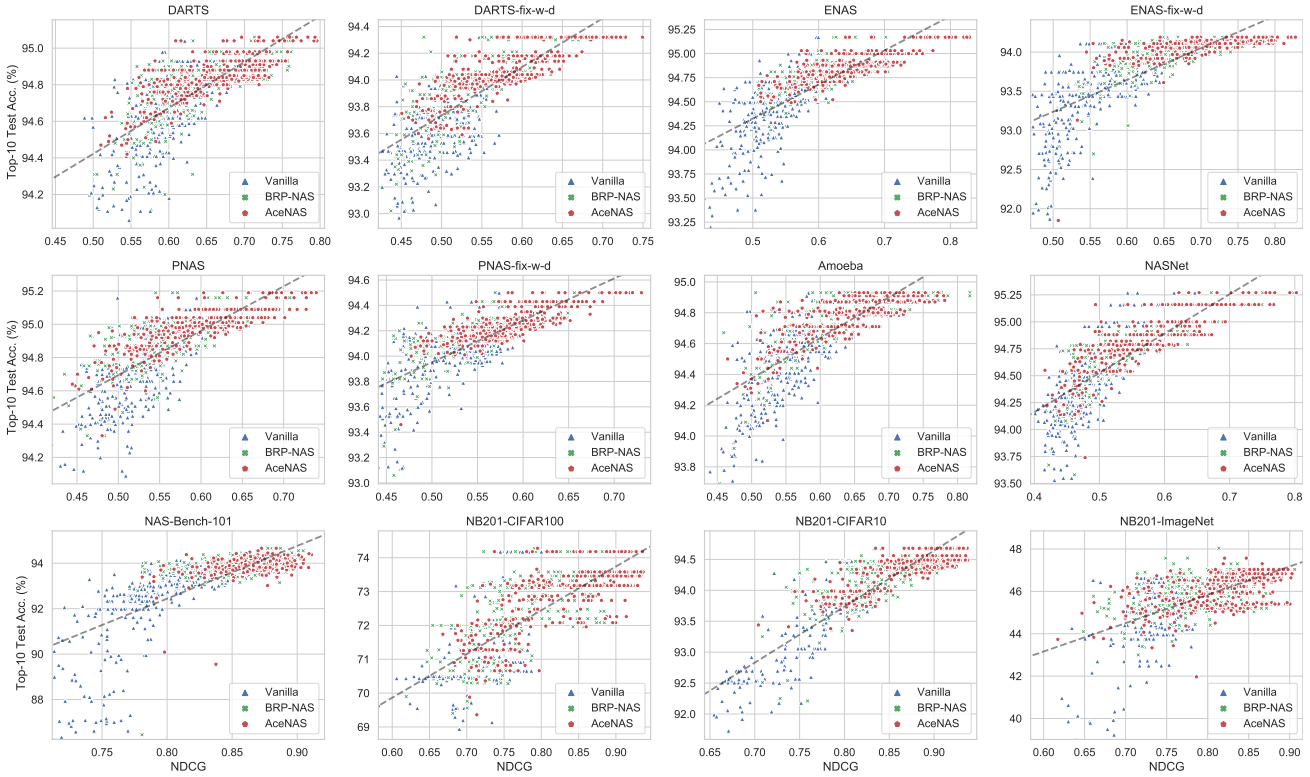


Figure E.3: AceNAS achieves better NDCG and accuracy on different search spaces. The upward trends show the correlation between NDCG and accuracy.

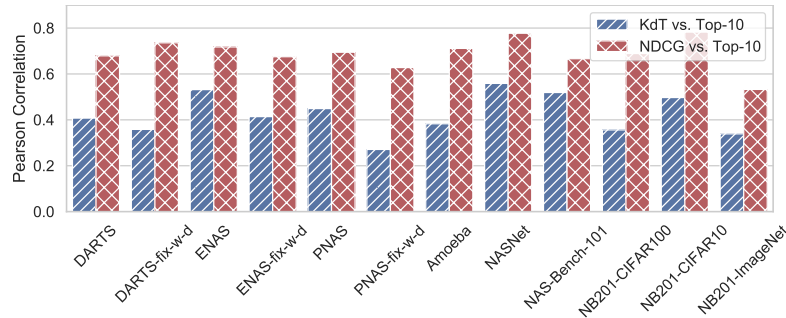


Figure E.4: Pearson correlation coefficients of different ranking metrics with respect to top-10 accuracy.

E.1.2 NDCG RELEVANCE SCORE

In this section, we study two important factors in Equation (8), and exploit different kinds of design choices. The experiment settings are the same as Section 5.2.1. We show the top-10 test regret (the gap between top-10 test accuracy and oracle test accuracy), and the total budget is fixed to 110.

We first compare different approaches to calculate upper bounds and lower bounds for normalization. Recall that, by default, the upper bound is the estimated with the maximum accuracy in the training samples, while the lower bound is the 20% quantile. Such strategy is compared with: (i) directly using minimum as lower bound; (ii) using 5%, 10% or 50% quantile as lower bound; (iii) using mean minus two times standard deviation as lower bound by assuming data to conform to a gaussian

distribution. The results are shown in Figure E.5, where we see that all the strategies perform similarly, except the minimum strategy which does not take outliers into consideration. The performance drop is particularly large on search spaces provided by NAS-Bench-201, where the accuracy distribution is highly skewed (see Figure B.1). Other than minimum, 50%-quantile also performs a little worse than others. We hypothesize that the ranking information of the bottom items is lost due to an over-aggressive clipping. As a result, the ranker fails to fully leverage all the data in training.

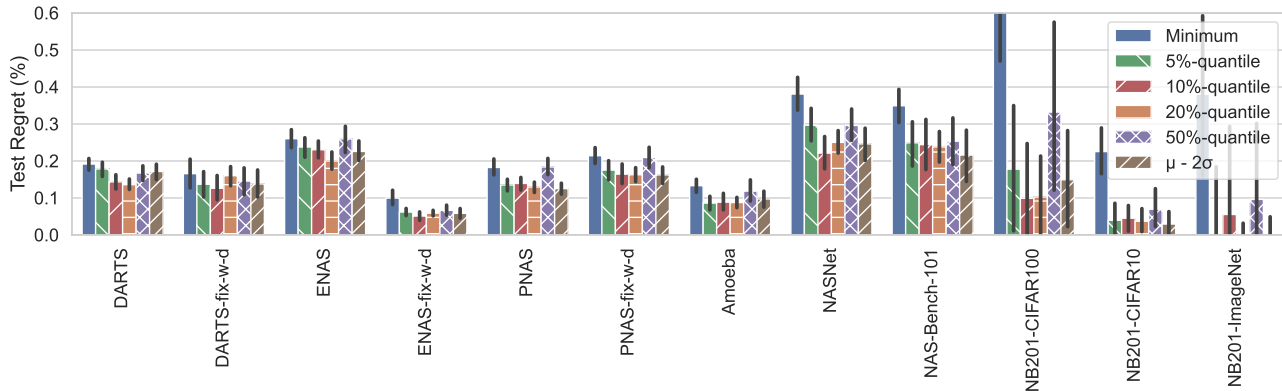


Figure E.5: Comparison of different methods to compute lower bound to normalize accuracies in NDCG computation.

We then compare different relevance scale, *i.e.*, S in Equation (8). By default $S = 20$. Other choices of S include 1, 2, 5, 10 and 50. We show the comparison in Figure E.6. Intuitively, higher S puts a higher emphasis on top-ranked architectures, which according to the claim of this paper, is more likely to produce higher performance. The experiment results show that this claim is generally true, except there is a slight performance drop when $S = 50$. We believe that the drop when $S = 50$ is because too large numbers used in the power of 2 result in numerical instability.

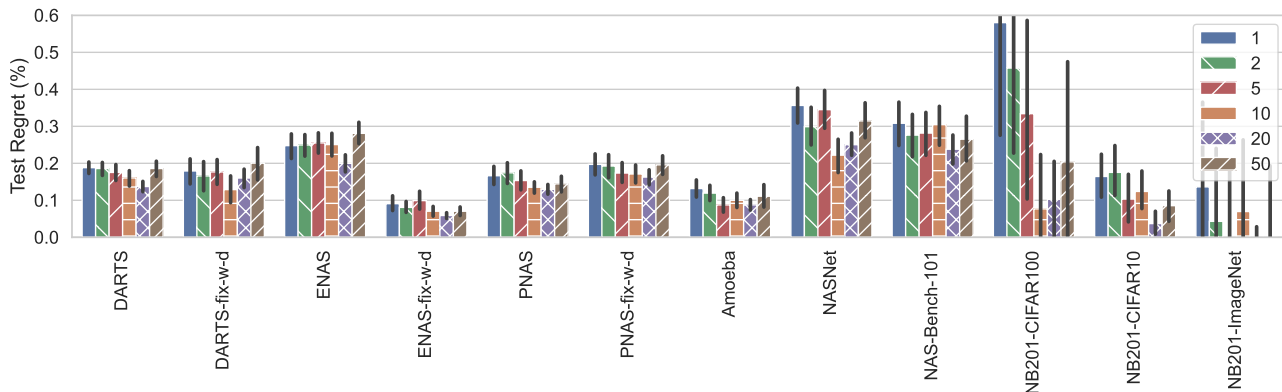
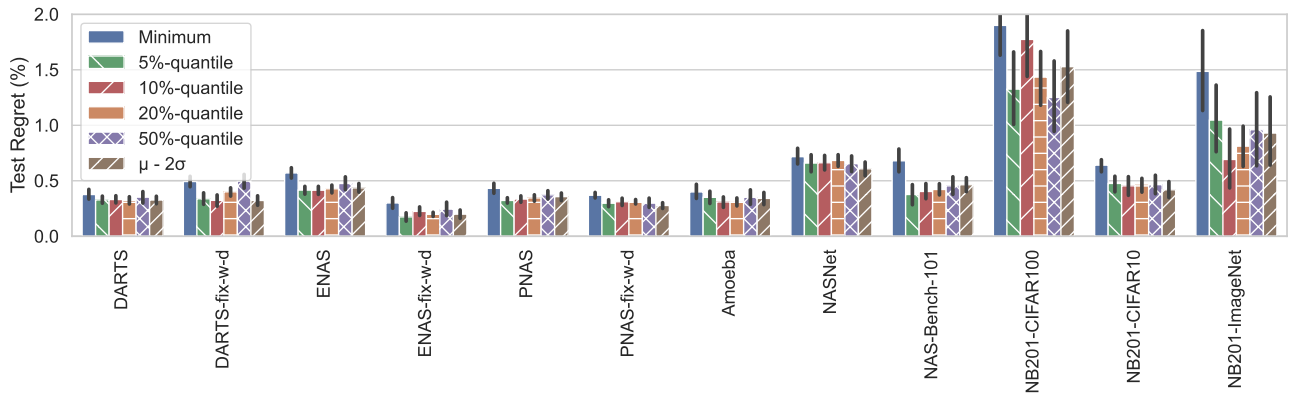


Figure E.6: Comparison of different relevance scales (S) in NDCG computation.

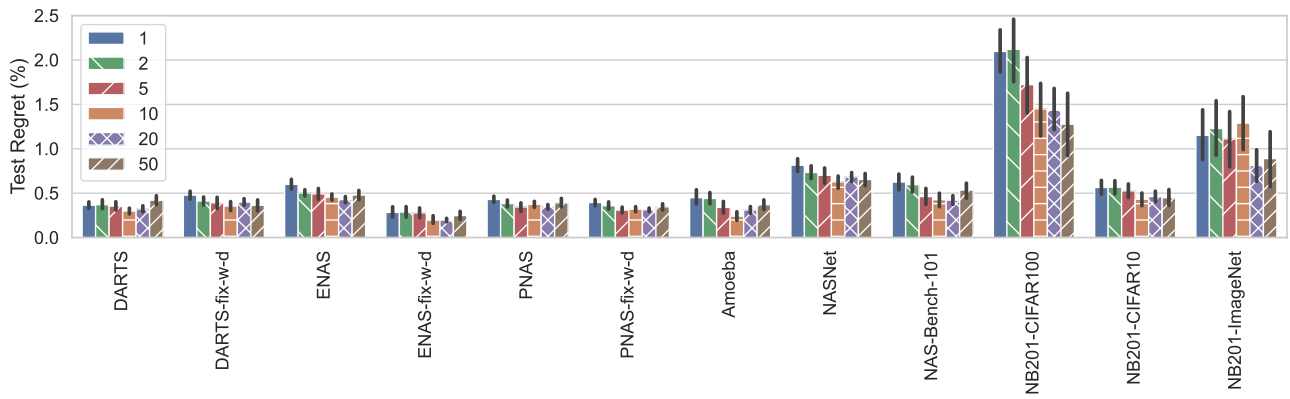
To verify whether Equation (8) still works well when the sampled architectures become fewer, we also repeat the experiments in Figure E.5 and Figure E.6 with a smaller budget (30). Intuitively, when the budget is smaller, the estimation of 20%-quantile is less accurate because it is calculated on fewer samples, but the overall conclusions are similar to what we have made with budget 110. The results are shown in Figure E.7.

E.2 Performance under different budgets

To show our effective under different budgets, we compare the highest accuracy of top-10 architectures returned by the ranker (*i.e.*, top-10 accuracy), and we repeat each experiment for 50 runs. We show the results in Figure E.8. On all 12 benchmarks, AceNAS consistently finds a better architecture than the two most-related GCN baselines (*i.e.*, Vanilla and BRP). Remarkably, AceNAS achieves higher accuracy than Vanilla (up to 0.62%) and BRP-NAS (up to 0.11%) under the smallest budget (*i.e.*, 20).



(a) Comparison of different methods to compute lower bounds.



(b) Comparison of different relevance scales.

Figure E.7: Comparison of different design choices in computing relevance scores, when budget is small (30).

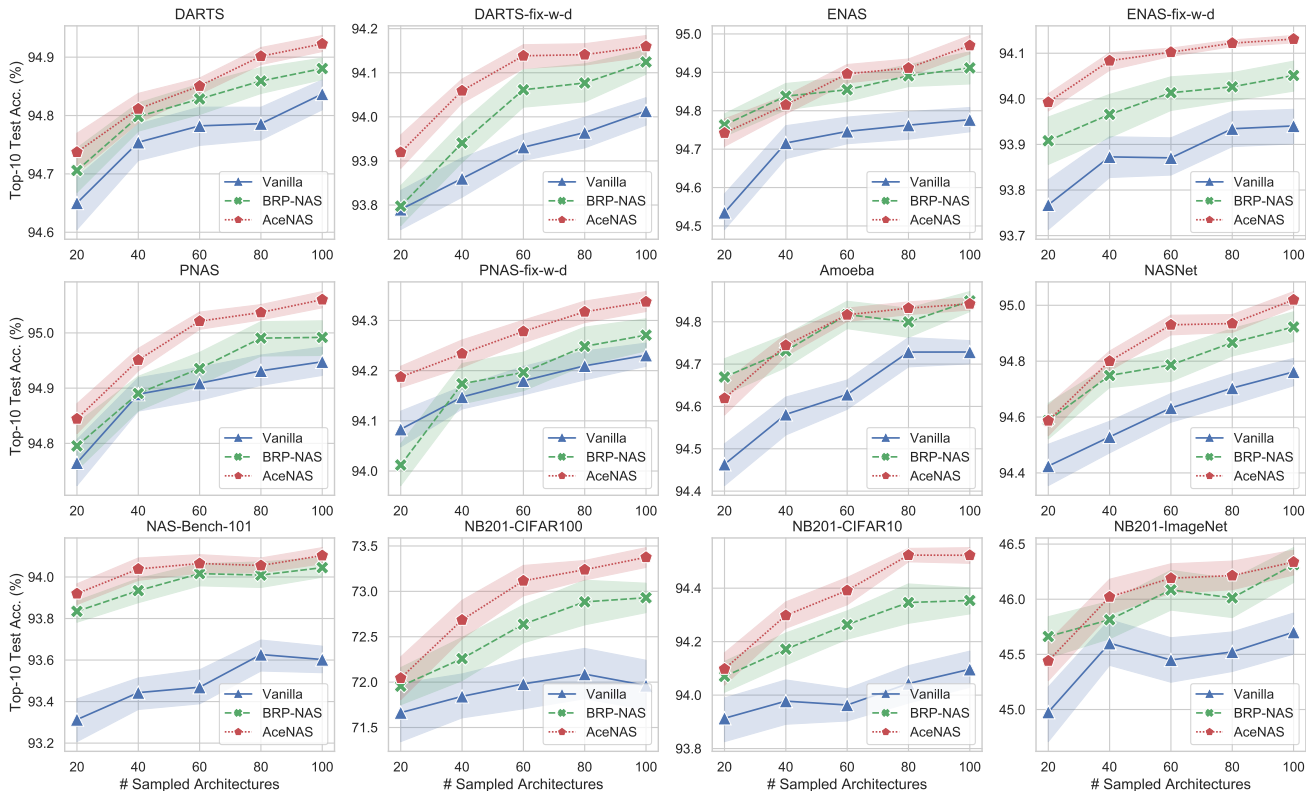


Figure E.8: AceNAS consistently surpasses Vanilla and BRP-NAS. Shaded regions here refer to 95% confidence interval. Please note that the number of samples on the x-axis does not take the final 10 samples (*i.e.*, top-10) into account.

E.3 Iterative sampling visualization

In Figure E.9, we visualize the whole process of AceNAS on NAS benchmarks. As the 100 architectures are iteratively sampled in 5 folds, we can see clear jumps on the curve at the point of 20, 40, 60, 80 and 100.

Given sufficient budgets, AceNAS can improve even more. In Figure E.10a, we search on NAS-Bench-101. With a total budget of 1000, we fine-tune the ranker when every 100 samples are collected. In Figure E.10b, we search on NAS-Bench-201 (CIFAR-100). We divide the total budget of 500 into 10 rounds (50 each). The accuracy bumps after the first round indicates the effectiveness of ranker on selecting good-performing architectures. Notably, on NAS-Bench-101, accuracy continues to improve after over 800 architectures are sampled. This result demonstrates that AceNAS is not likely to fall into local optimum despite fast convergence.

Similarly, we show the sampling process on ProxylessNAS search space. In Figure E.10c, we conduct 6 stages of evolution. In the first phase, 80 architectures are sampled, and in the rest stages, 30 stages on sampled. We guarantee all the architectures sampled satisfy our latency constraint.

E.4 More ablation study on ranking loss

We include the ablation study of ranking loss conditioned on multiple settings of pre-training, *i.e.*, no pre-training at all and pre-training with parameters and FLOPs. The results are shown in Figure E.11. We observe a consistent superiority that LambdaRank is better than RankNet, and RankNet is better than vanilla MSE loss.

E.5 AceNAS with different weight-sharing approaches

In Section 5.2.2, we combine AceNAS with 6 different weight sharing methods, and show the performance when each method is used to obtain the weak labels for AceNAS. In Table E.1, we show results on more search spaces. Note that we only run experiments on 6 instead of all 12 search spaces because supporting several methods on some of the search spaces are not straightforward (*e.g.*, NAS-Bench-101). The conclusions are similar to what we have made in Section 5.2.2. One extra observation is that, the performance of weight-sharing is highly related to the choice of search space. There is

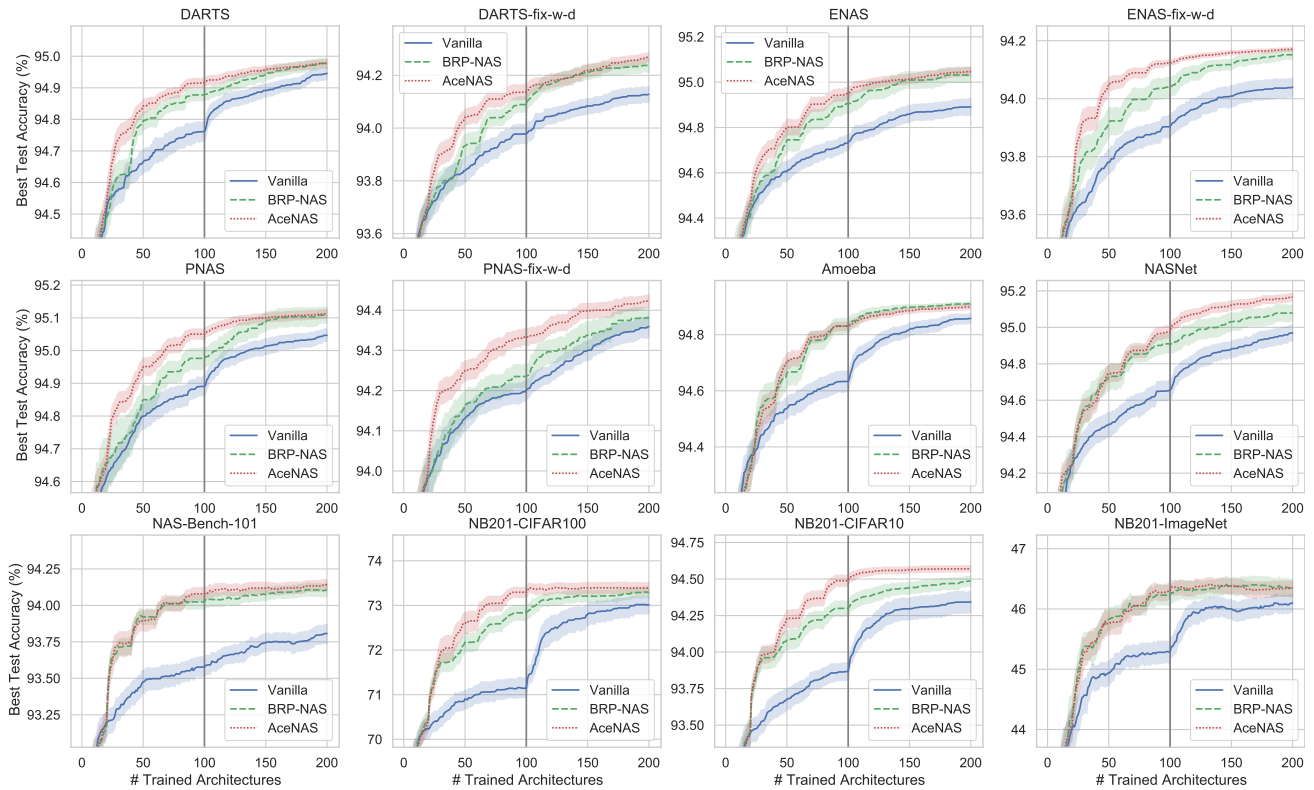
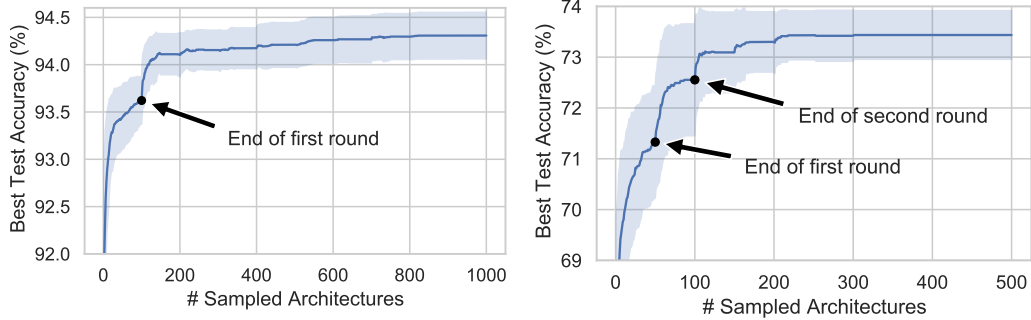
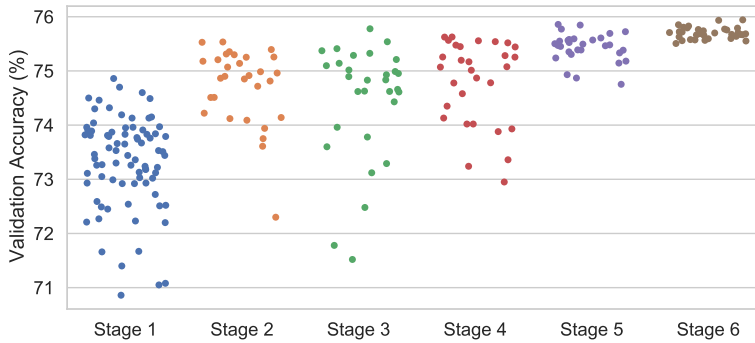


Figure E.9: The test accuracy of the architecture with best validation accuracy, with respect to number of architectures trained. After 100 architectures (the vertical black line), the ranker does not update any more. The budget of 100 architectures is splitted into 5 rounds. Each line is an average of 50 runs. The shaded regions are 95% confidence interval.



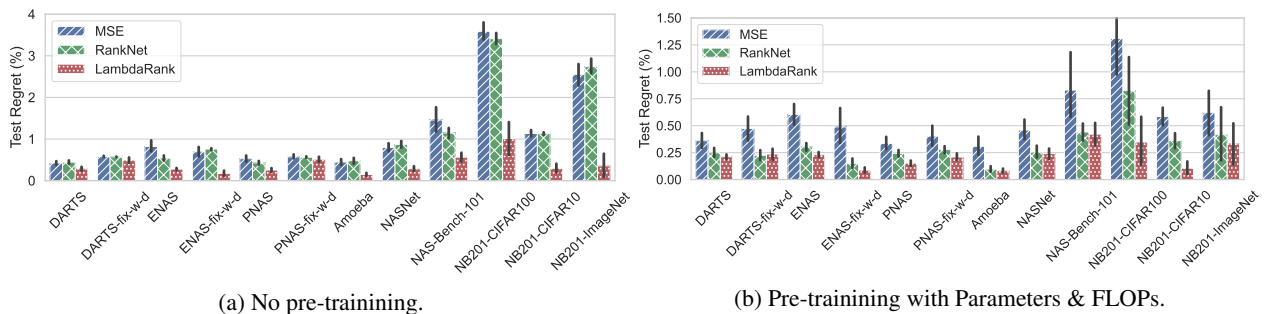
(a) NAS-Bench-101 (budget = 1000)

(b) NAS-Bench-201, CIFAR-100 (budget = 500)



(c) AceNAS optimization process on ProxylessNAS.

Figure E.10: On NAS-Bench-101 (left), with total budget of 1000, we update the ranker every 100 samples. The black dot denotes the first time ranker is updated. On NAS-Bench-201 (CIFAR-100) (right), with total budget of 500, we update the ranker every 50 samples. The black dots denote the first and second time ranker is updated.



(a) No pre-training.

(b) Pre-training with Parameters & FLOPs.

Figure E.11: Comparison among test regrets when using different LTR losses. **(left)**: when no pre-trainin is use. **(right)**: when pretraining with “Parameters and FLOPs” as weak labels. Each bar is an average of 50 runs.

no weight-sharing method that performs consistently well on all search spaces. This echoes the findings in (Zhang et al., 2020c).

Similar to Figure E.9, we visualize the iterative sampling process in Figure E.12 and compare the combination of AceNAS with different weight sharing NAS. It can be seen that the methods with a better starting point tend to have a better final performance. Another notable phenomenon is that on NAS-Bench-201-ImageNet, AceNAS + ENAS first finds an architecture with accuracy exceeding 46.5%, and then decreases to around 46.3%. This is a result of the discrepancy between validation accuracy and test accuracy, and the algorithm coincidentally finds an architecture that is good performing on test dataset.

Table E.1: Top-10 test accuracy when AceNAS is combined with weak labels obtained by different weight-sharing methods. Each number is an average of 50 runs. The best method in each column is highlighted with bold text, while the worst method is underlined.

Method	NB201-CIFAR100		NB201-CIFAR10		NB201-ImageNet		DARTS-fix-w-d		ENAS-fix-w-d		PNAS-fix-w-d	
	WS quality	AceNAS	WS quality	AceNAS	WS quality	AceNAS	WS quality	AceNAS	WS quality	AceNAS	WS quality	AceNAS
RandomNAS (Li & Talwalkar, 2019)	69.70	73.38	93.16	94.52	43.26	46.34	93.52	94.16	93.45	94.13	93.87	94.34
DARTS (1st order) (Liu et al., 2018)	73.44	73.40	94.45	94.57	45.10	46.51	94.14	94.30	<u>92.96</u>	94.11	94.13	94.33
DARTS (2nd order) (Liu et al., 2018)	<u>55.70</u>	<u>72.93</u>	<u>84.60</u>	94.46	<u>28.15</u>	46.19	93.80	94.12	93.56	<u>94.09</u>	94.08	<u>94.27</u>
FBNet (Wu et al., 2019)	70.01	73.40	93.96	94.51	41.49	46.30	<u>93.50</u>	94.10	94.10	93.13	94.12	<u>93.54</u>
ProxylessNAS (Cai et al., 2019b)	59.69	72.93	87.43	<u>94.44</u>	37.20	<u>45.97</u>	93.65	94.16	93.53	94.11	93.86	94.29
ENAS (Pham et al., 2018)	72.02	73.56	93.67	94.50	46.64	46.34	94.01	94.12	94.05	94.11	94.21	94.39

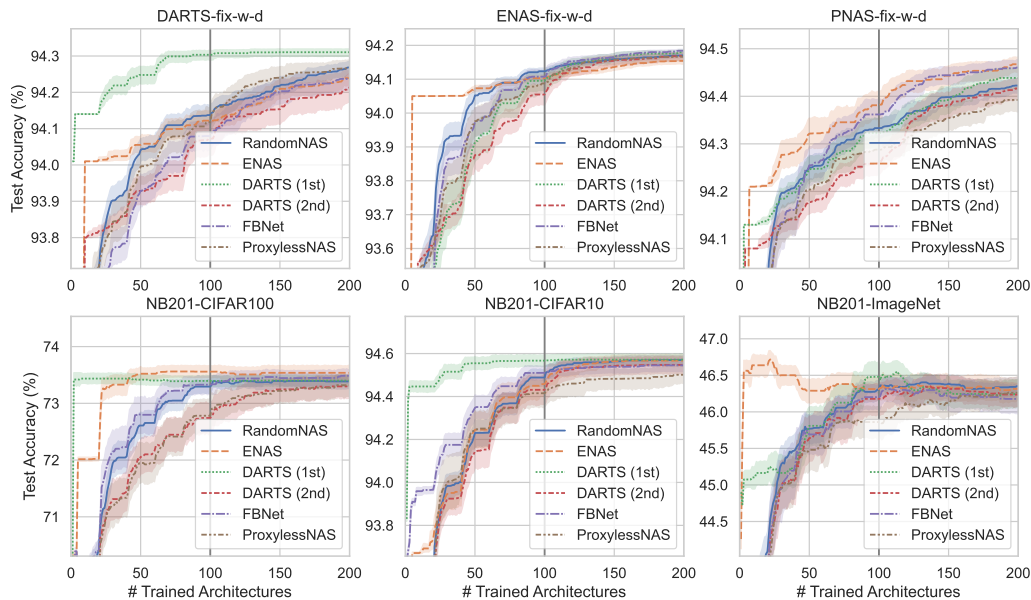


Figure E.12: Iterative sampling visualization of AceNAS + different weight sharing approaches. Settings resemble Figure E.9: first 100 samples are used to fine-tune the ranker, and the ranker itself is fixed after the vertical line.

E.6 AceNAS vs. pure weight-sharing

Another natural question is, would pure weight-sharing without AceNAS be competitive with AceNAS if they are given more budgets to fully train architectures? Here, we compare AceNAS against a “weight sharing guided search” (Pouchot et al., 2020) that selects top-100 architectures with the highest accuracy on weight-shared super-net. For fair comparison, AceNAS samples the same number of architectures. Specifically, 80 fully-trained architectures are iterative sampled, while the final ranking models predict the best 20 architectures. As shown in Figure E.13, AceNAS outperforms the weight-sharing based prediction. Remarkably, we reduce the test regret by 3% on NAS-Bench-201 (CIFAR-100). This experiment indicates that AceNAS is a necessary component, and weight-sharing alone does not work well.

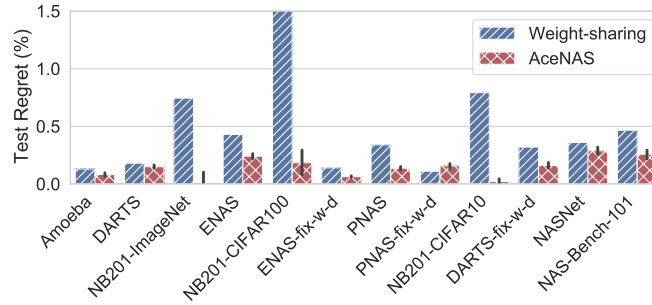


Figure E.13: Comparison of test regret between weight-sharing-guided greedy search and AceNAS on 100 budget.

E.7 Pretraining quality

In Figure E.14, we show how our ranker is good at capturing the information (*i.e.*, WS-accuracy, FLOPs and number of parameters) in the pretraining stage. Apart from 4k architectures that were used in training, we sampled extra 1k architectures per search space to evaluate the model. We compute R^2 scores (coefficient of determination), which can be as good as 1. We found that for parameters and FLOPs, our model hits > 0.98 for all search spaces, which means that the model is very good at predicting the model size. On WS-accuracy, R^2 scores vary between 0.4 and 1, implying that it always learn information from super-net, at least to some extent. Clearly, on some benchmarks (*e.g.*, NAS-Bench-101 and NAS-Bench-201), it looks better than others. We conjecture that search spaces with lower diversity (*e.g.*, spaces in NAS-Bench series) are easier to learn.

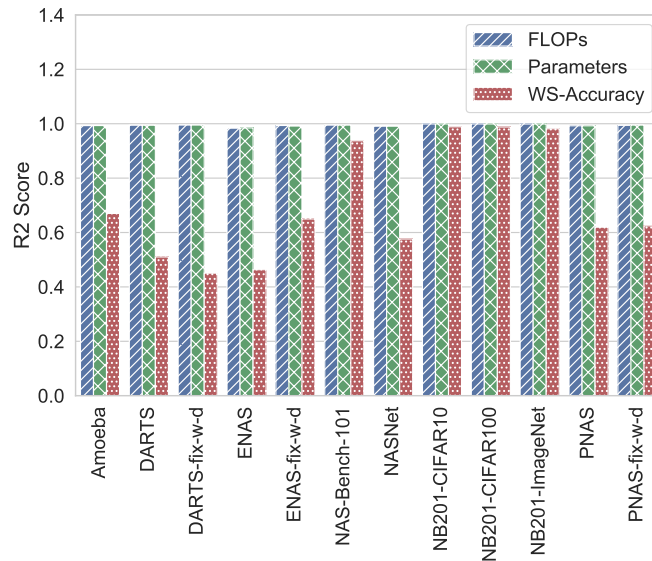


Figure E.14: The validation R^2 score in pretraining stage, indicating how good our ranker is good at predicting weight sharing accuracy, number of parameters and FLOPs.

E.8 Quality of searched architectures

For NAS benchmarks, we show in Table E.2 the test accuracy, test regret and rank of our searched architecture. *AceNAS* is approximately able to find the best architecture out of one thousand architectures. Remarkably, on NAS-Bench-201-ImageNet, it almost finds the best validation architecture on the search space (the negative test regret estimation is caused by variance). Despite that the best validation architecture has been located, it still ranks 2.14 out of 1000, which means that some architectures have a even better test accuracy, which is due to the gap between validation dataset and test dataset, and the best on validation is not necessarily the best on test.

For ProxylessNAS search space, we show the architectures found by 3 different runs, and name them AceNAS-M1, AceNAS-M2, and AceNAS-M3, respectively (M for Mobile). The network structures are shown in Figure E.15 and the accuracy and latency on ImageNet test set (commonly called validation set for historical reasons) are shown in Table E.3.

Table E.2: Test accuracy and rank of the best architecture, averaged over 50 runs. For test accuracy, we report the mean and standard deviation. For test regret and rank, we only report the mean. *: the gap between test accuracy of searched architecture and the best validation architecture. †: the average rank of test accuracy within all test accuracies.

Search space	Test acc.	Test regret*	Rank (%) †
NAS-Bench-101	94.10±0.20	0.24	0.33
NB201-CIFAR100	73.38±0.51	0.10	0.16
NB201-CIFAR10	94.52±0.15	0.04	0.05
NB201-ImageNet	46.34±0.56	-0.08	2.14
Amoeba	94.84±0.07	0.09	0.80
DARTS	94.92±0.07	0.14	1.20
DARTS-fix-w-d	94.16±0.12	0.16	1.00
ENAS	94.97±0.11	0.20	0.60
ENAS-fix-w-d	94.13±0.04	0.06	0.40
NASNet	95.02±0.15	0.25	0.41
PNAS	95.06±0.06	0.13	0.60
PNAS-fix-w-d	94.34±0.09	0.16	1.54

Pre-trained checkpoints of these models will be released.

Table E.3: Test accuracy and latency of architectures searched on ProxylessNAS (shown in Figure E.15).

Architecture	Test acc. (%)	Latency (ms)
AceNAS-M1	75.25	84.60
AceNAS-M2	75.07	84.59
AceNAS-M3	75.11	84.92

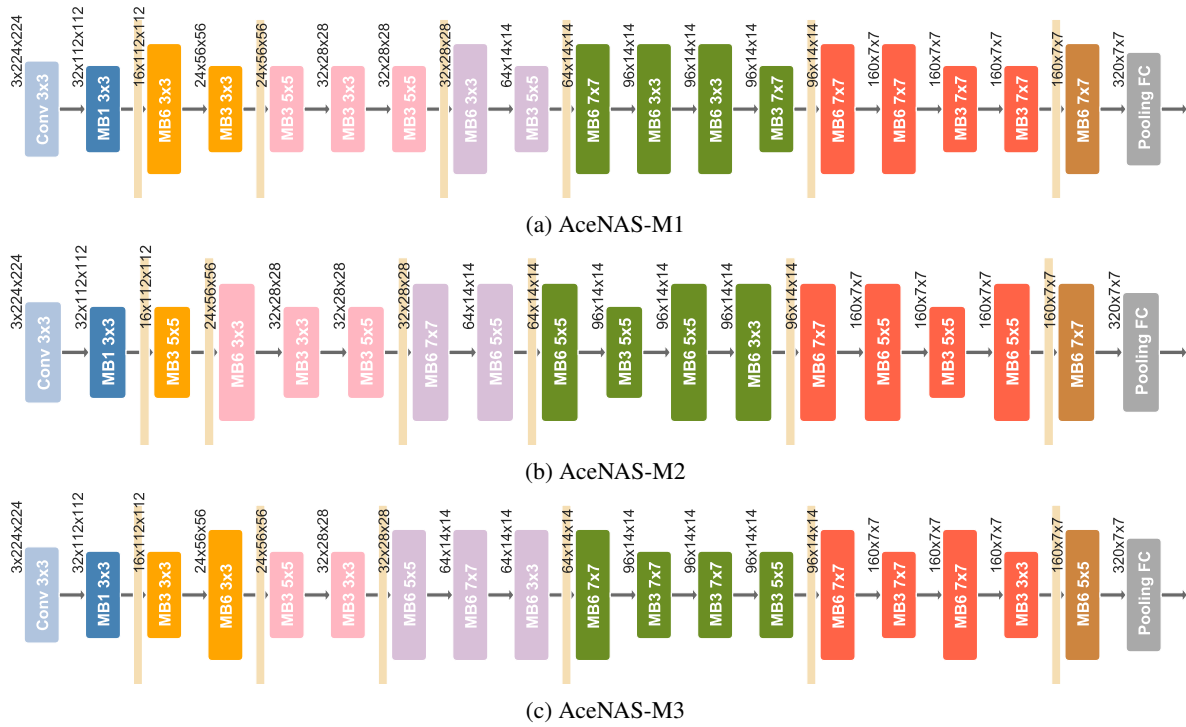


Figure E.15: Searched architecture on ProxylessNAS search space.